University of Stuttgart
Germany

Cross-over analysis of altimetry over ocean and investigating the orbital error's effect on inter-mission/track bias in inland altimetry

Oliver Kappich

Bachelor thesis
in the degree program **Geodäsie und Geoinformatik**
at the Institute of Geodesy, University of Stuttgart

Stuttgart, 01 2024

Supervisor: Dr.-Ing. Mohammad Tourian
Universität Stuttgart

GIS

Erklärung der Urheberschaft

Ich erkläre hiermit an Eides statt, dass ich die vorliegende Arbeit ohne Hilfe Dritter und ohne Benutzung anderer als der angegebenen Hilfsmittel angefertigt habe; die aus fremden Quellen direkt oder indirekt übernommenen Gedanken sind als solche kenntlich gemacht. Die Arbeit wurde bisher in gleicher oder ähnlicher Form in keiner anderen Prüfungsbehörde der Universität Stuttgart oder einer anderen Hochschule vorgelegt, und auch noch nicht veröffentlicht.

Ort, Datum

Unterschrift

Declaration of authorship

I declare in lieu of an oath, that the research reported within this thesis has been conducted by the author unless indicated otherwise. Ideas provided directly or indirectly by others have been marked for that. The material contained within this thesis has not previously been submitted for a degree to the examination authority of the University of Stuttgart or any other University, and is also not published otherwise.

Abstract

The largest part of Earth's surface (approximately 71%) is covered with water. Given the constantly changing environment, particularly amidst accelerated climate change, it is crucial to continuously measure the water levels of oceans and lakes. Therefore, satellite altimetry becomes essential.

The orbits of the altimetry satellites are selected in a way that allows satellites to pass over the same locations after a specific interval. These orbits are termed as repeat orbits, facilitating the creation of time series measurements. Over the past 40 years, numerous altimetry satellite missions have been launched. When multi-mission monitoring of water bodies is targeted, each satellite altimeter possesses its own biases, which should be removed for comparability among different missions. This ensures the creation of long-term data records by combining data from various missions. Over open oceans, this is typically achieved through a cross-calibration method. However, these methods prove effective for ocean data but not for inland altimetry.

In this thesis, I investigated the reasons for the bias among water values measured by different satellites. Additionally, I explored potential solutions to merge the data. The main focus lays on the tandem phases of Jason 1 and 2, as well as Jason 2 and 3. The study area focused on Lake Erie, situated in the Great Lakes region in the northwest of the US. To reduce the bias, I employed a cross-calibration method to estimate and reduce radial error components. As this approach does not resolve the entire bias problem, I investigated the retracking algorithms by comparing their results. Differences between height measurements of Jason 2 and Jason 3, both using MLE4, were identified. It could be determined that MLE4 in Jason 3 finds systematically lower values compared to Jason 2. Over the whole tandem phase, Jason 3 finds the retracking point approximately 20%, in respect to the leading edge, lower than Jason 2. The influence of this systematic difference on the SSH/LLH remains unclear, as no further investigations are done. To get a better understanding if the bias can be reduced when the mid-height point is used, two simple threshold retracking algorithms are employed. The outcome is, that the difference between Jason 2 and Jason 3 increased to 18.3 cm on average.
Lastly, I examined the corrections that need to be added to the range measurement of the satellite. This includes the geoid undulation, tidal height variations, the ocean surface response caused by atmospheric pressure and propagation delay due to the atmosphere. I found differences of 5 to 8 cm over Lake Erie in the atmosphere corrections. Employing the same corrections for two satellites yielded the most effective bias reduction. However, employing this technique, necessitates satellites passing the same location within a few minutes of each other. Consequently, the Jason satellites were selected during their tandem phases. On average the bias could be reduced from 7 cm to 2.4 cm.
The study delved into understanding and reducing biases in satellite altimetry measurements, particularly focusing on the tandem phases of Jason satellites, revealing

challenges and promising methods to significantly reduce biases.

Keywords: Altimetry satellites, water level, cross-calibration, retracking, time series, inland altimetry, repeat orbit

Contents

1 Introduction **1**
- 1.1 Radar Altimetry . . . 2
  - 1.1.1 Basic principle . . . 2
  - 1.1.2 Retracking . . . 4
  - 1.1.3 retracking methods . . . 7
- 1.2 Relevant missions . . . 7
  - 1.2.1 TOPEX series . . . 8
  - 1.2.2 ENVISAT . . . 9
  - 1.2.3 SARAL/AltiKa . . . 10
- 1.3 Problem statement . . . 10

2 Data and case study **13**
- 2.1 Data . . . 13
- 2.2 Case study . . . 14

3 Radial error estimation **15**
- 3.1 Methodology . . . 15
  - 3.1.1 Discrete modelling of radial errors . . . 15
  - 3.1.2 Least squares principle . . . 17
  - 3.1.3 Variance component estimate . . . 17
- 3.2 Procedure . . . 19
- 3.3 Results . . . 24

4 Bias analysis **31**
- 4.1 Time series during tandem phase of Jason satellites . . . 31
  - 4.1.1 Retracking investigations . . . 40
    - 4.1.1.1 Threshold retracking algorithm . . . 50
  - 4.1.2 Investigating corrections . . . 53

5 Summary and conclusions **63**

List of Figures

1.1 Aviso+ (2022). Timeline of modern radar altimetry missions. https://doi.org/10.24400/527896/A02-2022.001 version YYYY/MM 2
1.2 Shows satellite with Range (satellite to ocean surface), Altitude (distance between satellite and reference ellipsoid), Height (distance between reference ellipsoid and ocean surface) (*Jason-3 Products Handbook*, 2021) . . 3
1.3 Parts of a reflected waveform (Rosmorduc et al., 2011). 5
1.4 Concept of waveform retracking (Tourian, 2013). 6
1.5 Ground tracks of TOPEX series, SARAL/AltiKa and ENVISAT 8
1.6 Time series of Lake Erie 10

3.1 All radial error components of Jason 1 and ENVISAT of the first time span, displayed on a world map. 19
3.2 All radial error components of Jason 1 and ENVISAT of the first time span over time. 20
3.3 All radial error components of Jason 3 and SARAL/AltiKa of the first time span, displayed on a world map. 21
3.4 All radial error components of Jason 3 and SARAL/AltiKa of the first time span over time. 22
3.5 Track 152 of Jason 1, with all used radial error components, in red, along track. The searched radial errors over Lake Erie are marked in green. . . 23
3.6 The figure shows track 152 from Jason 1 cycle 010 and Jason 2 cycle 249 with radial errors removed. Each subplot shows the outcomes with different extrapolation methods 25
3.7 The figure shows track 152 from Jason 1 cycle 010 and Jason 2 cycle 249 with radial errors removed. Each subplot shows the outcomes with different extrapolation methods 26
3.8 The figure shows track 193 from Jason 1 cycle 010, Jason 2 cycle 249 and ENVISAT cycle 072 with radial errors removed. Each subplot shows the outcomes with linear, pchip and makima extrpolation methods 27
3.9 The figure shows track 152 from Jason 2 cycle 284 Jason 3 cycle 004 and SARAL/AltiKa cycle 032 with radial errors removed. Each subplot shows the outcomes with linear, pchip and makima extrpolation methods 29

4.1 Lake Erie LLH, Track 76 from Jason 1 cycle 252, Jason 2 cycle 013. On the top left are the reduced 1 Hz measurements, on the bottom left are the 20 Hz measurements. On the corresponding right side are maps that are showing the locations where the measurements are taken. 32

4.2 Lake Erie LLH, Track 152 from Jason 1 cycle 255, Jason 2 cycle 016. On the top left are the reduced 1 Hz measurements, on the bottom left are the 20 Hz measurements. On the corresponding right side are maps that are showing the locations where the measurements are taken. 33

4.3 Lake Erie LLH, Track 193 from Jason 1 cycle 249, Jason 2 cycle 010. On the top left are the reduced 1 Hz measurements, on the bottom left are the 20 Hz measurements. On the corresponding right side are maps that are showing the locations where the measurements are taken. 35

4.4 Lake Erie LLH, Track 76 from Jason 2 cycle 284, Jason 3 cycle 004. On the top left are the reduced 1 Hz measurements, on the bottom left are the 20 Hz measurements. On the corresponding right side are maps that are showing the locations where the measurements are taken. 36

4.5 Lake Erie LLH, Track 152 from Jason 1 cycle 281, Jason 2 cycle 001. On the top left are the reduced 1 Hz measurements, on the bottom left are the 20 Hz measurements. On the corresponding right side are maps that are showing the locations where the measurements are taken. 37

4.6 Lake Erie LLH, Track 193 from Jason 1 cycle 288, Jason 2 cycle 008. On the top left are the reduced 1 Hz measurements, on the bottom left are the 20 Hz measurements. On the corresponding right side are maps that are showing the locations where the measurements are taken. 39

4.7 The figure is showing cutouts of the waveforms reflected from Lake Erie, during the tandem phase of Jason 1 and Jason 2. It shows cutouts of one overflight over Lake Erie (track 193). The brightness symbolises the signal amplitude. The graphic is divided by the red line. On left are the waves of Jason 1, on the right are the waves from Jason 2. The x-axis shows the total number of waves. The red points are the retracked points of Jason 1 with MLE4 algorithm. The blue and cyan ones are the retracking points, MLE3 and MLE4, of Jason 2. 41

4.8 The graphic shows the retracking points of Jason 1 and Jason 2. These are the same points as in Figure 4.7, in better presentation to be compared. 42

4.9 The figure is showing cutouts of the waveforms reflected from Lake Erie, during the tandem phase of Jason 2 and Jason 3. It shows cutouts of one overflight over Lake Erie (track 193). The brightness symbolises the signal amplitude. The graphic is divided by the red line. On left are the waves of Jason 3, on the right are the waves from Jason 2. The x-axis shows the total number of waves. The red and green points are the retracked points of Jason 3, MLE4 and MLE3. The blue and cyan ones are the retracking points, MLE3 and MLE4, of Jason 2. 43

4.10 The graphic shows the retracking points of Jason 2 and Jason 3. These are the same points as in Figure 4.9, in better presentation to be compared. 44

4.11 The two histograms display the location of the retracking point, with respect to the leading edge, in percentage. The leading edge is defined as the first peak, with an signal amplitude greater than 100, of the waveform. In the special case, that the the location of the retracking point is above the leading edge, the maximal peak of the waveform is used for the leading edge. Both plots are created by using MLE4 retracking. The histogram on the top, belongs to Jason 2. The histogram on the bottom, belongs to Jason 3. The Histograms are made of all measurements over Lake Erie, that are observed during the whole tandem phase of Jason 2 and Jason 3 at track 76. 45

4.12 The two histograms display the location of the retracking point, with respect to the leading edge, in percentage. The leading edge is defined as the first peak, with an signal amplitude greater than 100, of the waveform. In the special case, that the the location of the retracking point is above the leading edge, the maximal peak of the waveform is used for the leading edge. Both plots are created by using MLE4 retracking. The histogram on the top, belongs to Jason 2. The histogram on the bottom, belongs to Jason 3. The Histograms are made of all measurements over Lake Erie, that are observed during the whole tandem phase of Jason 2 and Jason 3 at track 152. 47

4.13 The two histograms display the location of the retracking point, with respect to the leading edge, in percentage. The leading edge is defined as the first peak, with an signal amplitude greater than 100, of the waveform. In the special case, that the the location of the retracking point is above the leading edge, the maximal peak of the waveform is used for the leading edge. Both plots are created by using MLE4 retracking. The histogram on the top, belongs to Jason 2. The histogram on the bottom, belongs to Jason 3. The Histograms are made of all measurements over Lake Erie, that are observed during the whole tandem phase of Jason 2 and Jason 3 at track 193. 48

4.14 The graphic is showing boxplots, one of each histogram shown in Figure 4.11, 4.12 and 4.13, of the percentages of the height of the retracking point from the first peak height (if its greater than 100%, the maximal peak height is used) of each wave. The top and bottom of each box are the 75th and 25th percentiles of the data. The red line inside the box is the median of the data. The Whiskers are the dotted lines from the box to the furthest observations. The red '+' are outliers (*Visualize summary statistics with box plot*, 2006). 49

4.15 Example of a waveform over Lake Erie from Jason 2. The first and max peak, as defined by thr50f and thr50max, are marked in red. 50

4.16 LLH of Lake Erie during tandem phase of Jason 2 and 3, using thr50f and thr50max. LLH from Jason 3 cycle 004. For Jason 2 the same corrections from Jason 3 are used. 51

4.17 Corrections provided from Jason 2 (blue) cycle 288 and Jason 3 (red) cycle 008 for track 193, GDR products. Between the two green lines Lake Erie is located. 53
4.18 Lake Erie LLH, Track 76 from Jason 1 cycle 252, Jason 2 cycle 013. On the top left are the reduced 1 Hz measurements, on the bottom left are the 20 Hz measurements. On the corresponding right side are maps that are showing the locations where the measurements are taken. The corrections which were used for Jason 1 and Jason 2, are from the Jason 1 GDR-E product. 54
4.19 Lake Erie LLH, Track 152 from Jason 1 cycle 255, Jason 2 cycle 016. On the top left are the reduced 1 Hz measurements, on the bottom left are the 20 Hz measurements. On the corresponding right side are maps that are showing the locations where the measurements are taken. The corrections which were used for Jason 1 and Jason 2, are from the Jason 1 GDR-E product. 55
4.20 Lake Erie LLH, Track 193 from Jason 1 cycle 249, Jason 2 cycle 010. On the top left are the reduced 1 Hz measurements, on the bottom left are the 20 Hz measurements. On the corresponding right side are maps that are showing the locations where the measurements are taken. The corrections which were used for Jason 1 and Jason 2, are from the Jason 1 GDR-E product. 57
4.21 Lake Erie LLH, Track 76 from Jason 2 cycle 284, Jason 3 cycle 004. On the top left are the reduced 1 Hz measurements, on the bottom left are the 20 Hz measurements. On the corresponding right side are maps that are showing the locations where the measurements are taken. The corrections which were used for Jason 3 and Jason 2, are from the Jason 3 GDR-F product. 58
4.22 Lake Erie LLH, Track 76 from Jason 2 cycle 281, Jason 3 cycle 001. On the top left are the reduced 1 Hz measurements, on the bottom left are the 20 Hz measurements. On the corresponding right side are maps that are showing the locations where the measurements are taken. The corrections which were used for Jason 3 and Jason 2, are from the Jason 3 GDR-F product. 59
4.23 Lake Erie LLH, Track 193 from Jason 2 cycle 288, Jason 3 cycle 008. On the top left are the reduced 1 Hz measurements, on the bottom left are the 20 Hz measurements. On the corresponding right side are maps that are showing the locations where the measurements are taken. The corrections which were used for Jason 3 and Jason 2, are from the Jason 3 GDR-F product. 61

List of Tables

1.1 Orbit characteristics of TOPEX series (*OSTM/Jason-2 Products Handbook*, 2017) 9
1.2 Orbit parameters of ENVISAT and SARAL/AltiKa (*Envisat Overview*, n.d.; Aviso+, n.d.) 9
1.3 This table shows the differences in [cm] of the lake level between the satellites. It shows the differences of the means and the medians. For this calculations the values from Figure 1.6 are used. The means/medians are formed only during the time where both satellites work simultaneously. Here its always row minus column. 11

2.1 Data products used in this thesis 13

3.1 Results of different extrapolation methods. The measurements come from track 152 from Jason 1 cycle 010 and Jason 2 cycle 249. The first row shows the results without any radial errors removed to the LLH. 24
3.2 Results of different extrapolation methods. The measurements come from track 152 from Jason 1 cycle 010 and Jason 2 cycle 249. The first row shows the results without any radial errors removed to the LLH. 26
3.3 Results of different extrapolation methods. The measurements come from track 152 from Jason 2 cycle 284, Jason 3 cycle 004 and ENVISAT cycle 032 track 0996. The first row shows the results without any radial errors removed to the LLH. At the column **Δmedian** the differences are always formed in the following order: Jason 1 - Jason 2; Jason 1 - ENVISAT; Jason 2 - ENVISAT 28
3.4 Results of different extrapolation methods. The measurements come from track 152 from Jason 2 cycle 284, Jason 3 cycle 004 and SARAL/AltiKa cycle 032 track 0452. The first row shows the results without any radial errors removed to the LLH. At the column **Δmedian** the differences are always formed in the following order: Jason 3 - Jason 2; Jason 3 - SARAL/AltiKa; Jason 2 - SARAL/AltiKa 30

4.1 The table lists the wet and dry troposheric corrections, as well as the ionospheric correction that are used, unless otherwise is noted; ECMWF: European Center for Medium Range Weather Forecasting; JMR: Jason Microwave Radiometer; AMR: Advanced Microwave Radiometer; MWR: Microwave Radiometer 31

4.2 Mean, median and standard deviation (std) of 1 Hz measurements, which are visualized in Figure 4.1, 4.2 and 4.3. At the column **Δmedian** the differences are always formed in the following order: Jason 1 - Jason 2 MLE4; Jason 1 - Jason 2 MLE3; Jason 2 MLE4 - Jason 2 MLE3. Acronyms: Jason 1 (J1), Jason 2 (J2), track (t.), cycle (c.) 34
4.3 Mean, median and standard deviation (std) of 20 Hz measurements, which are visualized in Figure 4.1, 4.2 and 4.3. At the column **Δmedian** the differences are always formed in the following order: Jason 1 - Jason 2 MLE4; Jason 1 - Jason 2 MLE3; Jason 2 MLE4 - Jason 2 MLE3. Acronyms: Jason 1 (J1), Jason 2 (J2), track (t.), cycle (c.) 34
4.4 Mean, median and standard deviation (std) of 1 Hz measurements, which are visualized in Figure 4.4, 4.5 and 4.6. Jason 3 MLE4 serves as the reference mission for the differences. Acronyms: Jason 3 (J3), Jason 2 (J2), track (t.), cycle (c.) 38
4.5 Mean, median and standard deviation (std) of 20 Hz measurements, which are visualized in Figure 4.4, 4.5 and 4.6. Jason 3 MLE4 serves as the reference mission for the differences. Acronyms: Jason 3 (J3), Jason 2 (J2), track (t.), cycle (c.) 38
4.6 The table is showing the mean, median and the standard deviation (std) of the retracking bins of track 193 from Jason 1 cycle 249 and Jason 2 cycle 010. The bins are also visualized in the Figure 4.7 and 4.8 41
4.7 The table is showing the mean, median and the standard deviation (std) of the retracking bins of track 193 from Jason 2 cycle 284 and Jason 3 cycle 004. The bins are also visualized in the Figure 4.9 and 4.10 43
4.8 The table is showing the mean, median and standard deviation (std.) of the data shown in Figure 4.16. 52
4.9 Mean, median and standard deviation (std) of 20 Hz measurements, which are visualized in Figure 4.18, 4.19 and 4.20. For the measurements of Jason 2, the corrections from Jason 1 are used. At the column **Δmedian** the differences are always formed in the following order: Jason 1 - Jason 2 MLE4; Jason 1 - Jason 2 MLE3; Jason 2 MLE4 - Jason 2 MLE3. Acronyms: Jason 1 (J1), Jason 2 (J2), track (t.), cycle (c.) 56
4.10 Mean, median and standard deviation (std) of 20 Hz measurements, which are visualized in Figure 4.18, 4.19 and 4.20. For the measurements of Jason 2, the corrections from Jason 1 are used. At the column **Δmedian** the differences are always formed in the following order: Jason 1 - Jason 2 MLE4; Jason 1 - Jason 2 MLE3; Jason 2 MLE4 - Jason 2 MLE3. Acronyms: Jason 1 (J1), Jason 2 (J2), track (t.), cycle (c.) 56
4.11 Mean, median and standard deviation (std) of 20 Hz measurements, which are visualized in Figures 4.4, 4.5 and 4.6. For the measurements of Jason 2, the corrections from Jason 3 are used. Jason 3 MLE4 serves as the reference mission for the differences. Acronyms: Jason 3 (J3), Jason 2 (J2), track (t.), cycle (c.) 60

4.12 Mean, median and standard deviation (std) of 20 Hz measurements, which are visualized in Figure 4.4, 4.5 and 4.6. For the measurements of Jason 2, the corrections from Jason 3 are used. Jason 3 MLE4 serves as the reference mission for the differences. Acronyms: Jason 3 (J3), Jason 2 (J2), track (t.), cycle (c.) 60

Chapter 1

Introduction

Radar satellite altimetry stands as a breakthrough in Earth observation, notably within the realm of studying marine and inland water dynamics. This cutting-edge technology leverages radar instruments aboard orbiting satellites to intricately measure surface elevations, providing unprecedented insights into the ever-changing nature of our planet's oceans, seas, and inland waterways. With its ability to precisely assess sea levels, track oceanic currents, and survey the topography of ice-covered regions, radar altimetry has evolved into an indispensable tool for comprehending the intricacies of Earth's aquatic ecosystems.

Moreover, this technology showcases versatility that extends beyond oceans, enabling precise measurements of water levels in inland lakes. This capability significantly contributes to evaluating water resource management strategies, monitoring ecosystem health, and contributing to broader regional climate studies. By seamlessly integrating radar technology with satellite capabilities, radar satellite altimetry remains pivotal in unraveling vital information about global water systems. Its contributions empower scientific research, facilitate environmental monitoring efforts, and offer diverse practical applications.

Accompanying the narrative, Figure 1.1 provides a comprehensive overview of radar altimetry missions spanning from past to future missions, illustrating their operational timelines.

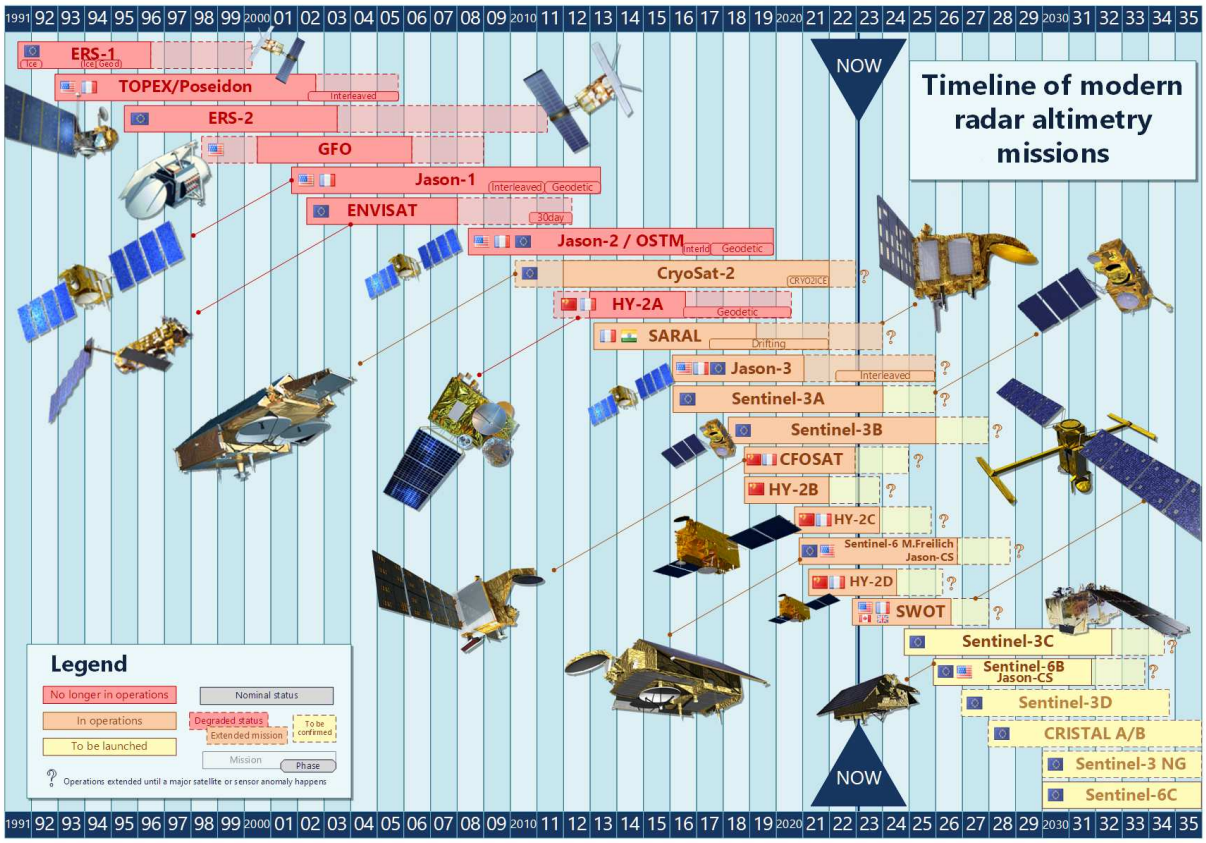

Figure 1.1: *Aviso+ (2022). Timeline of modern radar altimetry missions. https://doi.org/10.24400/527896/A02-2022.001 version YYYY/MM*
(*Aviso+ (2022). Timeline of modern radar altimetry missions.*, 2022)

1.1 Radar Altimetry

1.1.1 Basic principle

The fundamental principle of satellite altimetry involves measuring the distance R between the satellite and the sea surface. To perform this measurement, the satellite is equipped with an altimeter that operates using electromagnetic radiation. It emits a brief pulse directed toward the sea surface, which interacts with and reflects the signal back to the satellite.
The primary method for measuring the range involves determining the time taken for the signal to travel from the satellite to the sea surface and back. Additionally, since the speed of light is a known constant, this leads to the following formula, equation (1.1).

$$\hat{R} = \frac{c \cdot t}{2} \tag{1.1}$$

In the formula above equation (1.1) the atmospheric effects are neglected. In order to take these into account, corrections have to be applied to $\hat{R}$. Considering those corrections leads to formula equation (1.2).

$$R = \hat{R} + \sum_j \Delta R_j \tag{1.2}$$

A reference ellipsoid, that approximates the geoid, is used to determine the altitude H of the satellite above the reference ellipsoid. The height h of the sea surface, relative to the reference ellipsoid can then be determined equation (1.3).

$$h = H - R \tag{1.3}$$

An overview is shown in Figure 1.2. There, R is labeled as Range, h the height of the sea surface and H is labeled as Altitude.

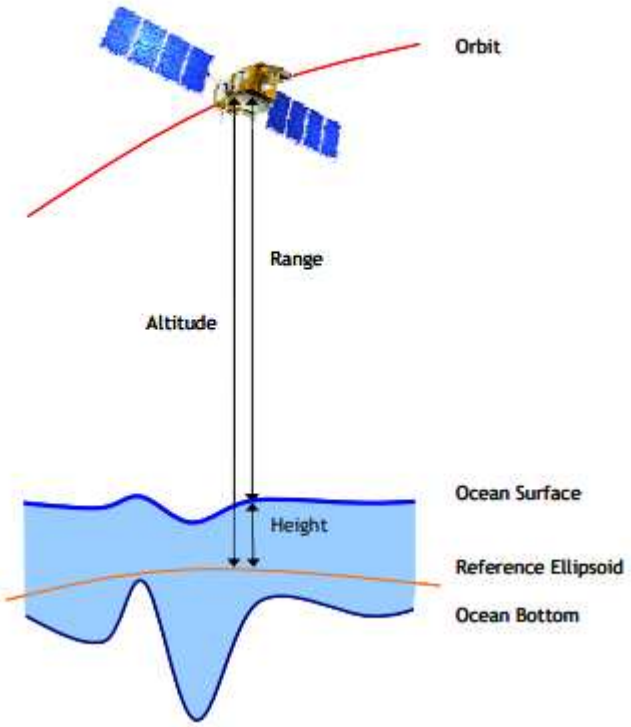

Figure 1.2: *Shows satellite with Range (satellite to ocean surface), Altitude (distance between satellite and reference ellipsoid), Height (distance between reference ellipsoid and ocean surface)* (Jason-3 Products Handbook, *2021)*

To compare different sea surface heights accurately, several geophysical effects must be accounted for and corrected. These effects include the geoid undulation h_g, tidal height variations h_T, and the ocean surface response h_a caused by atmospheric pressure. The sea surface height is then described as a result of these adjustments.

$$h_{SSH} = h - h_g - h_T - h_a \tag{1.4}$$

The sea surface height (SSH) as described in equation (1.4) is used for the research in this thesis (Fu and Cazenave, 2000).

1.1.2 Retracking

Retracking is a crucial process in satellite altimetry used to determine the precise location of the sea surface from the received radar echoes. It's important because it helps in extracting accurate information about sea levels, ocean currents and inland lake level heights.
The primary objective of retracking is to analyze the radar echoes returned by the surface to pinpoint the range between the satellite and the sea or lake surface. However, several challenges and sources of error can affect the accuracy of retracking. One significant challenge arises from the complex nature of the radar return signal, which can be influenced by surface roughness, wind conditions, and interference from various sources. Incorrect retracking can lead to misinterpretation of the signal, resulting in inaccuracies in determining the sea surface height or lake level height.
Moreover, environmental conditions such as changing wind speeds or wave heights can impact the shape of the returned radar echoes, making it challenging to identify the exact point representing the sea or lake surface. This uncertainty in retracking can introduce errors in the final measurements, affecting the precision of the data collected by altimetry satellites.
Therefore, while retracking is vital for extracting valuable information from satellite altimetry data, its accuracy is essential to mitigate errors and ensure reliable interpretations of the measurements and that's why it is discussed here.

For each range measurement a pulse is emitted and the reflection of it will be received. The echo over the ocean can be outlined with an averaged waveform, as shown in Figure 1.3 (Rosmorduc et al., 2011).

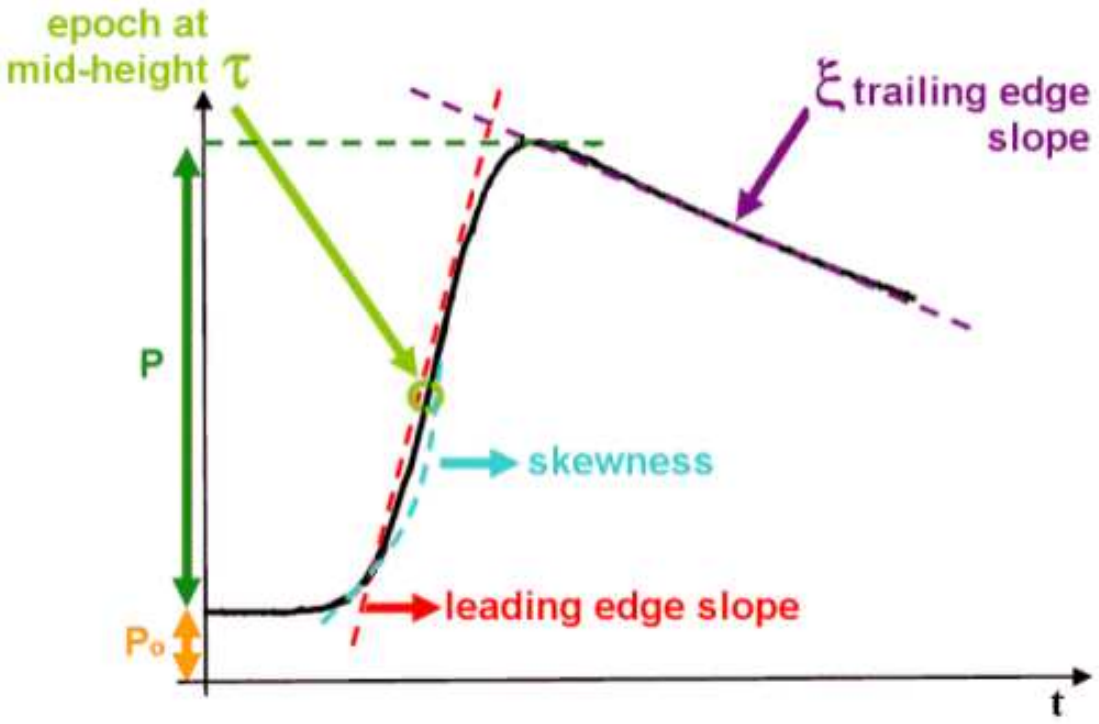

Figure 1.3: *Parts of a reflected waveform (Rosmorduc et al., 2011).*

Figure 1.3 contain some key parameters:

- epoch at mid-height: is the time used to figure out how long it takes for the radar pulse to travel from the satellite to the surface and back again. This time delay is estimated by a tracker algorithm.
- P: amplitude of the signal
- P_0: thermal noise
- skewness: leading edge curvature
- trailing edge slope: this is linked to any mispointing of the antenna (Rosmorduc et al., 2011).

The range can be estimated out of the time the pulse travelled. For this, a certain point on the waveform must be defined as the water surface. In many cases the mid-height point on the leading edge is chosen. Thus, retrackers try to estimate this point.

In practise, an offset between the mid-height point of the leading edge of the waveform (*retracking gate*) and a predetermined, consistent, and instrument-independent point on the leading edge, known as the *tracking gate* (Figure 1.4) occurs. Within the altimeter, this offset indicates an error in the measurements of the range and waveform retracking involves using a specific algorithm to determine this offset (Tourian, 2013). Further descriptions of these retracking algorithms are below (Section 1.1.3), as they are used for the investigations I made.

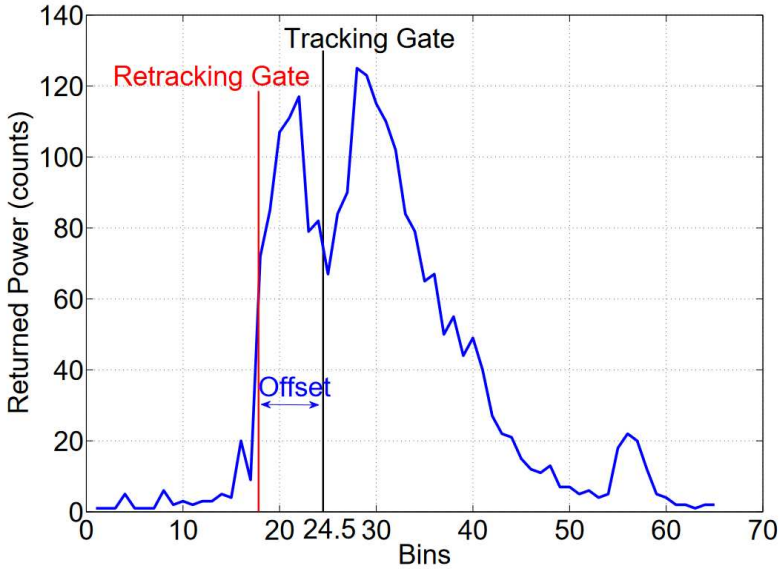

Figure 1.4: *Concept of waveform retracking (Tourian, 2013).*

Retracking is the processing step to find the epoch at mid-height. Thus, the tracker offset can be determined and finally the range can be computed (Rosmorduc et al., 2011).
The bin of the retracking gate can be determind as follows:

$$bin = \frac{2 \cdot (r_{Ku} - r_t)}{3.125\text{ns} \cdot c_0} + 32 \tag{1.5}$$

- r_{Ku}: range measurement from K_u-band.
- r_t: tracker range.
- 3.125ns: sample sensitivity of Jason satellites.
- c_0: speed of light in vacuum. $c_0 = 299792458 \frac{\text{m}}{\text{s}}$ (Wikipedia, 2023)
- $+32$: add bin of tracker, which is 32 for Jason satellites, to the bin difference.

1.1.3 retracking methods

To locate the mid-height point accurately, various methods of retracking exist. Some of them will be described here, as they are employed for retracking in this thesis.

- **Threshold**: As the names says a threshold is defined, here at 50%. The threshold is in respect to the amplitude of the leading edge or through an alternative definition. An used methodology relies on rectangle dimensions calculated through the OCOG method, which identifies the center of gravity for each waveform by based on the power levels within the gates. This approach is a entirely statistical approach. Threshold values are anchored here to a wanted percentage of the amplitude relative to the OCOG amplitude or the maximum waveform amplitude. The selection of the retracking gate is determined by linear interpolation between neighboring samples that cross the steep part of the leading edge of the threshold. The simpler *thr50max* and *thr50f*, described in 4.1.1.1, are not using the OCOG method. They search the amplitude of the leading edge or waveform and apply a 50% threshold to it.
- **Physically-based**: Such retrackers are based on the theoretical knowledge of microwave scattering at nadir. An often used waveform model is the Brown ocean waveform model (Figure 1.3). The average return power as a function of time delay (t) for a rough scattering surface, can be expressed as a convolution of three terms:

$$W(t) = FSSR(t) * PTR(t) * PDF(t) \tag{1.6}$$

  where *FSSR* is the flat sea surface response, PTR is the radar point target responses and PDF is the ocean surface elevation probability density function of specular points (Vignudelli et al., 2011).

Another important step is to fit the model to the actual waveform. Thus, the retracking gate can be estimated more precisely. An important method is the *Maximum Likelihood Estimator* (MLE). The variants MLE3 and MLE4 of it are used in Jason 1, 2 and 3. Thereby, a different number of unknowns of the waveform model must be solved. For the MLE3 it is the range, the backscatter coefficient (σ_0) and the significant wave height (SWH). The MLE4 retracking algorithms estimates the 4 parameters range, SWH, the backscatter coefficient (σ_0) and the square of mispointing angle (ξ^2) (Vignudelli et al., 2011; *Jason-1 Products Handbook*, 2016; *OSTM/Jason-2 Products Handbook*, 2017; *Jason-3 Products Handbook*, 2021).

1.2 Relevant missions

In this section the satellites I used in this thesis are introduced. The used satellites are from the TOPEX series (Jason 1, Jason 2 and Jason 3), ENVISAT and SARAL/AltiKa. Looking at the ground tracks the differences of the orbits getting visible (Figure 1.5). ENVISAT and SARAL/AltiKa have a much denser ground pattern than the TOPEX

orbit. More details of the different missions and their orbit characteristics are described below (Section 1.2.1, 1.2.2 and 1.2.3).

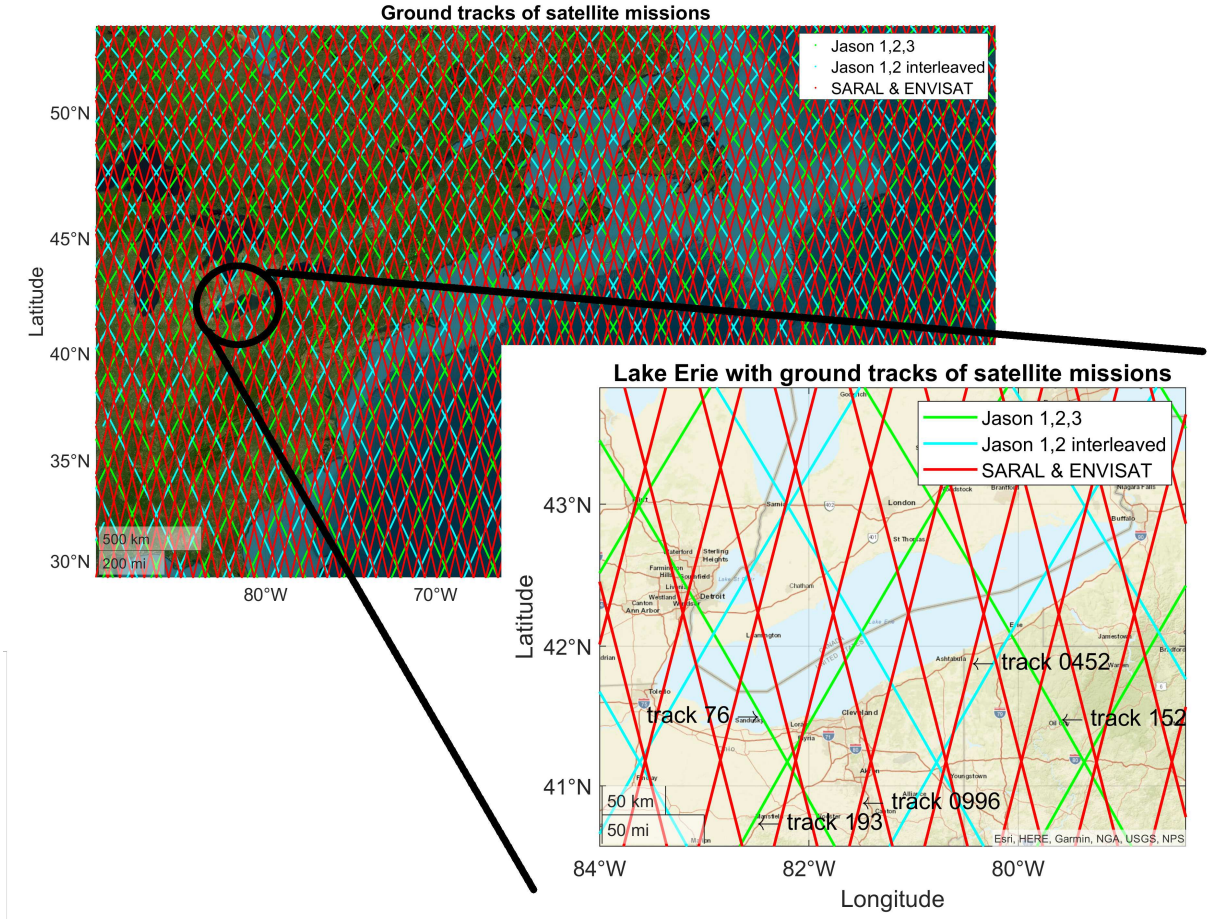

Figure 1.5: *Ground tracks of TOPEX series, SARAL/AltiKa and ENVISAT*

1.2.1 TOPEX series

The TOPEX series comprises all satellites utilizing the identical orbit to TOPEX/Poseidon. In my thesis, I used Jason 1-3. Following the launch of Jason 2, Jason 1 and Jason 2 entered a tandem phase. Throughout this phase, both satellites traversed the same orbit with 1 minute apart. Subsequently, Jason 1 was transitioned to an interleaved orbit, and a similar adjustment was made for Jason 2 and Jason 3. Table 1.1 includes some of the most critical orbit parameters (*OSTM/Jason-2 Products Handbook*, 2017; *Jason-3 Products Handbook*, 2021).

Table 1.1: *Orbit characteristics of TOPEX series (*OSTM/Jason-2 Products Handbook*, 2017)*

Semi-major axis (a)	7714.432 km
Eccentricity (e)	0.000098
Inclination (I)	66.042°
Longitude of the ascending node (Ω)	116.56°
Argument of perigee (ω)	90.0°
Mean anomaly (M)	253.13°
Longitude of equator crossing of pass 1	99.9242°
(Equatorial) Altitude above reference ellip.	1339.65 km
Repeat cycle	9.9156 days

The orbit of Jason 1 and Jason 2 changed into an interleaved orbit during their operational time. The longitude of the first equator crossing changed to 98.51°.(*Jason-1 Products Handbook*, 2016; *OSTM/Jason-2 Products Handbook*, 2017).

1.2.2 ENVISAT

In March 2002, the European Space Agency launched Envisat, an advanced satellite for Earth observation. It conducted measurements of the atmosphere, ocean, land, and ice. Envisat's sophisticated payload continued the data collection legacy of ESA's ERS satellites, aiding Earth science research and monitoring environmental and climatic changes. The gathered data also supported various operational and commercial applications. Alongside its predecessors ERS-1 and ERS-2, Envisat significantly expanded our understanding of Earth sciences and facilitated applications for environmental monitoring.
The nominal phase orbit was changed for the mission extension phase in October 2010. Some basic orbit parameters are shown in Table 1.2. Over its 10-year span, Envisat orbited Earth more than 50,000 times, doubling its intended lifetime. The mission produced a vast amount of data, which were instrumental in studying Earth's systems and offering insights into factors contributing to climate change (*Envisat Overview*, n.d.).

Table 1.2: *Orbit parameters of ENVISAT and SARAL/AltiKa (*Envisat Overview*, n.d.; Aviso+, n.d.)*

Semi major axis (a)	7159.496 km
Eccentricity (e)	0.000165
Inclination (I)	98.55°
Argument of perigee (ω)	90.0°
Longitude of equator crossing of pass 1	0.1335°
Mean altitude above reference ellip.	799.8 km
Repeat cycle	35 days

1.2.3 SARAL/AltiKa

From its launch in February 2013 until July 2016, SARAL/AltiKa maintained a repetitive orbit. The SARAL mission has been a pivotal element of the altimetry constellation since 2013, reclaiming the long-standing ground track established by previous missions like ERS and ENVISAT. Thus it has the same orbit characteristics as ENVISAT (Table 1.2). From July 2016, the repetitive ground track was no longer maintained, causing the orbit to naturally drift due to decay. The SARAL satellite, operated by the Indian Space Research Organization (ISRO) and equipped with the AltiKa altimeter (operating at Ka-band, 35 GHz) developed by CNES, also includes a Doris instrument. The utilization of signal frequencies in the Ka-band allows for improved observations of various phenomena such as ice, rain, coastal zones, land masses (such as forests), and wave heights.
Furthermore, SARAL/AltiKa represents the initial showcase of Ka-band altimeter capabilities for precise resolution along-track applications, particularly beneficial for studying coastal and inland water regions (Aviso+, n.d.).

1.3 Problem statement

With satellite altimetry, time series of water bodies can be obtained. In general, there will be a bias between the measurements of different satellite missions (Figure 1.6). In order to bring those measurements together an often used method is a cross-calibration. This allows to create long term time series including several different satellite missions.

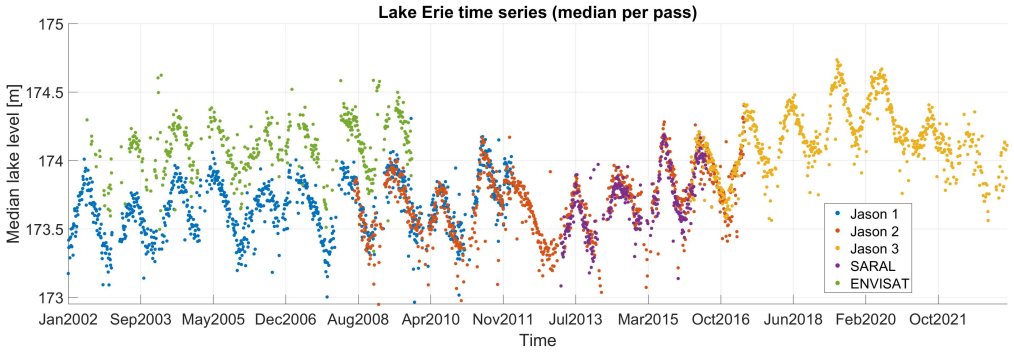

Figure 1.6: *Time series of Lake Erie*

The problem of biases between different missions, is visualized in Figure 1.6. It shows Lake Erie, an inland lake in the USA. Lake Erie is used in the case study (Chapter 2). A bias between Jason 1 and ENVISAT is obvious. Also a difference between Jason 2 and SARAL/AltiKa is visible. In this figure the data of ENVISAT and SARAL/AltiKa is not shown for their complete lifespan.
Below in Table 1.3 the biases are listed.

Table 1.3: *This table shows the differences in [cm] of the lake level between the satellites. It shows the differences of the means and the medians. For this calculations the values from Figure 1.6 are used. The means/medians are formed only during the time where both satellites work simultaneously. Here its always row minus column.*

	Jason 1	Jason 3	SARAL/AltiKa	ENVISAT
Jason 2	mean: -5.4 cm median: -5.4 cm	mean: -4.6 cm median: -4.1 cm	mean: 3.5 cm median: 4.8 cm	mean: -47.5 cm median: -43.2 cm
ENVISAT	mean: 44.8 cm median: 45.1 cm			

It is noticeable that the differences between the Jason satellites are way lower than the differences that involve ENVISAT or SARAL/AltiKa. This might be, as the Jason satellites used theirs predecessor for calibration and validation (*OSTM/Jason-2 Products Handbook*, 2017).
In this thesis, I investigated the source of the bias and in order to minimize the bias, I used a cross-calibration method (Section 3). As this turned out to be unsuccessful, I did comparisons with different retracking algorithms and looked for differences between the results (Section 4.1.1). Moreover, I investigated the corrections that are provided in the different products of the satellites (Section 4.1.2).

Chapter 2

Data and case study

2.1 Data

The satellite data is provided by different institutions, such as *Aviso+* operated by the french space agency CNES. Another institution is EUMETSAT, an intergovernmental organisation with 30 member states. Both provide the *Geophysical Data Record* (GDR), which comes in different versions. The versions are numbered alphabetically. Starting with first version "A" and the latest version "F" for Jason 2 and 3 as well as for SARAL/AltiKa, version "E" for Jason 1. The latter "T" is reserved for calibration/validation version. The GDR contains the native products which includes sea surface height, ocean surface wind speed, significant wave height information and all required corrections. The versions may differ for example in the orbit models, the provided retracking algorithms, models for tidal corrections and so on. An additional expert sensor format (S-GDR) also contains the full radar-echo waveforms (*Jason-1 Products Handbook*, 2016; *SARAL/AltiKa Products Handbook*, 2021).
The ENVISAT enhanced processing Level 2 for RA-2 instrument I used, belongs also to the GDR products, but without alphabetical numbering (Benveniste and Milagro, 2000).
The Table 2.1 lists all data product I used in this thesis.

Table 2.1: *Data products used in this thesis*

Mission	**Product**
ENVISAT	enhanced, Level-2, RA-2
Jason 1	GDR-E and SGDR-E
Jason 2	GDR-D and SGDR-D
Jason 3	GDR-F and SGDR-F
SARAL/AltiKa	GDR-F

2.2 Case study

To investigate the error, that cause the bias between different satellites, a case study is made. For the case study the area of Lake Erie is chosen. Lake Erie is located in the north-east of the USA, at the Great Lakes region. There are several reasons for the choice of Lake Erie. First Lake Erie is sufficiently large enough for satellite altimetry. As satellite radar altimeter footprints can have several kilometers in diameter (*Sentinel-3 SRAL Marine User Handbook*, 2017) and additionally several measurements during one overflight should be done. This results in the need of a large body of water. Another reason is that several different satellite altimetry mission overfly Lake Erie several times each repeat cycle, so the lake level can be measured at different locations with different satellites. Figure 1.5 shows the ground tracks of the used missions over Lake Erie.
In this chapter, the main focus lays on finding the source of the bias. The Jason series is predestinated, as during the tandem phases two satellites are flying on the exact same orbit with approximately 70 seconds (*OSTM/Jason-2 Products Handbook*, 2017) and 56 seconds (*Jason-1 Products Handbook*, 2016) apart. This ensures that the circumstances for the measurement, like the lake level height and atmosphere, are the same for both satellites.

Chapter 3

Radial error estimation

In this chapter, radial errors are determined and added to the satellite measurements. Radial errors consists of orbital errors, errors in geophysical correction models, time tagging errors, etc.

3.1 Methodology

A crossover point of a mission, is the point where an ascending and a descending track are intersecting. For two different missions any intersection, creates a crossover point. The methodology employed in this study is based on Bosch et al. (2014).
The crossover analysis for computation is divided into 10-day segments, each overlapping by 2 days with its neighboring periods.

3.1.1 Discrete modelling of radial errors

For the discrete modelling, radial error components, r_i and r_j, are introduced at every crossover point. The two passes are marked by i and j. For both tracks a time for the crossing, t_i and t_j, are introduced as well. For every crossover point the difference of the sea surface height h can be determined:

$$\Delta x_{ij} = h_i - h_j$$

If the time gap between both passes at a crossover point exceeds two days, the crossover point is excluded from consideration.
The crossover differences are modelled by the difference of two radial error components with residuals.

$$\Delta x_{ij} + e_{ij} = r_i - r_j$$

This is done for every crossover, which leads to a linear system of equations for n crossover differences.

$$\boldsymbol{\Delta} + \boldsymbol{e_B} = \boldsymbol{B^T} \cdot \boldsymbol{r} \tag{3.1}$$

Notice that there are two times more radial errors $\boldsymbol{r^T} = (r_1, r_2, ..., r_{2n})$ than crossover differences. This leads to the $n \times 2n$ coefficient matrix:

$$\boldsymbol{B^T} = \begin{bmatrix} +1 & 0 & \cdots & 0 & -1 & 0 \\ 0 & 0 & +1 & -1 & 0 & 0 \\ \vdots & \vdots & \vdots & \vdots & \vdots & \vdots \\ 0 & +1 & \cdots & 0 & 0 & -1 \end{bmatrix} \tag{3.2}$$

The position of derivations depends on the sorting in the linear equation system equation (3.1). $\boldsymbol{\Delta}$ is weighted as follows:

$$\boldsymbol{W}_B = \frac{1}{\sigma_B^2} \boldsymbol{P}_B \tag{3.3}$$

with $\boldsymbol{P}_B$ as an diagonal matrix. Each weight is set up as follows:

$$p_{ij}(\Delta t_{ij}) = \frac{\sigma_0^2}{\sigma_\Delta^2} \cdot \frac{\delta t_B^2}{\delta t_B^2 + \Delta t_{ij}^2} \cdot cos(\phi) \tag{3.4}$$

- σ_0: unit weight std., is set to 0.01m.
- σ_Δ: standard differences of the crossover differences. Std. for each track (3 SSH values, around crossover, in each direction) and error propagation of difference.
- δt_B: half weight width, set to 0.3 days.
- Δt_{ij}^2: time difference of overflights.
- ϕ: latitude

Since there are more unknowns than equations in the linear system equation (3.1), a constraint must added. Thus the differences of consecutive errors are added as new "observations".

$$0 + e_{i,i+1} = r_i - r_{i+1}$$

Thereby, $2n - 1$ equations are added. This can be written in matrix notation as well:

$$\boldsymbol{0} + \boldsymbol{e} = \boldsymbol{D^T} \cdot \boldsymbol{r} \tag{3.5}$$

When ordering the error components strictly in time, the $2n - 1 \times 2n$ coefficient matrix looks then as follows:

$$\boldsymbol{D^T} = \begin{bmatrix} +1 & -1 & 0 & \cdots & \cdots & 0 \\ 0 & +1 & -1 & \cdots & \cdots & 0 \\ \vdots & \ddots & \ddots & \ddots & \ddots & \vdots \\ 0 & \cdots & 0 & +1 & -1 & 0 \\ 0 & \cdots & \cdots & 0 & +1 & -1 \end{bmatrix} \tag{3.6}$$

The weights are defined by:

$$\boldsymbol{W}_m = \frac{1}{\sigma_m^2}\boldsymbol{P}_m \tag{3.7}$$

with mission $m = 1, \ldots, N$. This implies that each mission has its own weighting. The combination leads to $\boldsymbol{W}_D$.

Consecutive errors (equation (3.5)) shall be applied only for the same satellite. To keep radial error components ordered in time and separate the constraint by missions, a sufficiently large time offset is added and after the adjustment removed.

$$t_i^{(m)} = t_i + (m-1) \cdot \Delta T \tag{3.8}$$

- ΔT: time offset

Due to the time offset for each mission, $\boldsymbol{D^T}$ has a block structure.

3.1.2 Least squares principle

Now, the least squares minimization can be applied. The new coefficient matrix is made up as follows:

$$\boldsymbol{M} = \begin{bmatrix} \boldsymbol{B^T} \\ \boldsymbol{D^T} \end{bmatrix}, \text{ the right hand side } \boldsymbol{d} = \begin{bmatrix} \boldsymbol{\Delta} \\ \boldsymbol{0} \end{bmatrix}$$

The system still has a rank defect. Thus, the constraint $\boldsymbol{k^T r} = 0$, where $\boldsymbol{k}$ is a vector with only one non zero element is introduced. With this constraint one equation in the linear system can be solved and the rank defect is gone.
The weight shall be combined as well.

$$\boldsymbol{W} = \begin{bmatrix} \boldsymbol{W_B} & \boldsymbol{0} \\ \boldsymbol{0} & \boldsymbol{W_D} \end{bmatrix} \tag{3.9}$$

The derivation is not described in this thesis (see Bosch et al. (2014)). The least squares are given by:

$$\hat{\boldsymbol{r}} = (\boldsymbol{M^T W M} + \boldsymbol{k k^T})^{-1} \boldsymbol{B W_B \Delta} \tag{3.10}$$

3.1.3 Variance component estimate

A variance component estimation is added, to ensure an objective relative weighting between all missions that are included. With this iterative procedure the variance factors, σ_B^2 and σ_m^2 for missions $m = 1, \ldots, N$, can be estimated.
With

$$\boldsymbol{Q = M^T W M + k k^T}$$

the partial redundancies can be computed by:

$$r_B = n_B - \boldsymbol{tr}(\frac{1}{\sigma_B^2} \boldsymbol{B P_B B^T Q^{-1}}) \tag{3.11}$$

$$r_m = n_m - \boldsymbol{tr}(\frac{1}{\sigma_m^2} \boldsymbol{D_m^T P_m D_m Q^{-1}}) \tag{3.12}$$

The new variance components can be estimated as follows:

$$\hat{\sigma}_B^2 = \frac{\boldsymbol{e_B^T P_B e_B}}{r_B} \tag{3.13}$$

$$\hat{\sigma}_m^2 = \frac{\boldsymbol{e_m^T P_m e_m}}{r_m} \tag{3.14}$$

The weight matrices (equation (3.3) and equation (3.7)) can be recalculated now.

3.2 Procedure

As mentioned above in Section 3.1, the crossover adjustment is divided in 10-day segments. The computation is split into two parts during the tandem phases of the Jason satellites. The first set of radial errors covers all crossovers from September 1, 2008 to December 1, 2008. This covers a part of the tandem phase of Jason 1 and 2. Additionally, ENVISAT operated at the same time. The second set of radial errors covers all crossovers from April 1, 2016 to July 1, 2016. This time span covers a part of the tandem phase of Jason 2 and 3. SARAL/AltiKa worked at the same time.
After the crossover adjustment, the radial error components at the crossover points are estimated. Since, only crossover points over the ocean are used, the radial error components are also over the ocean (Figure 3.1).

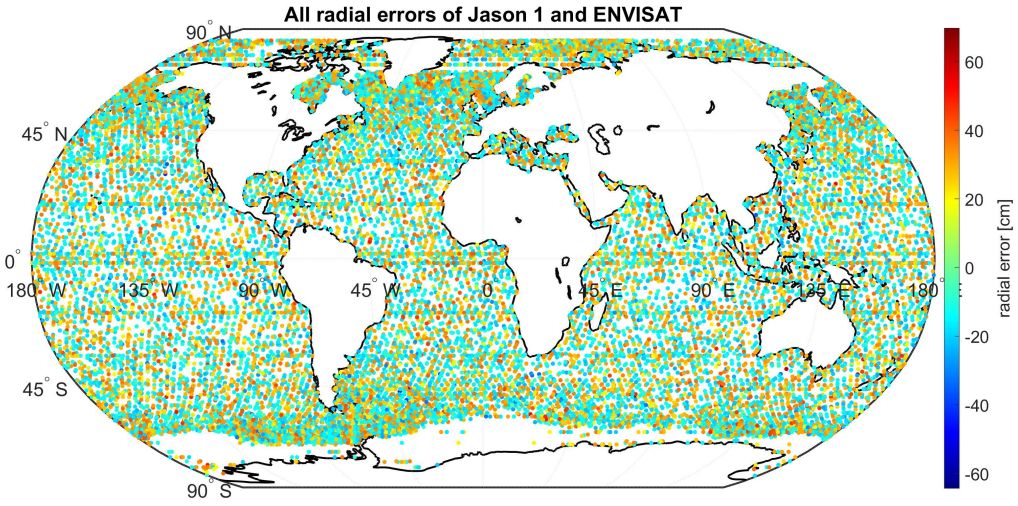

Figure 3.1: *All radial error components of Jason 1 and ENVISAT of the first time span, displayed on a world map.*

In Figure 3.1 one can see that the radial errors are relative evenly distributed. Most of the radial errors are in a range of ±20 cm. Some outliers are also visible, but there is no geographic related pattern.

Nevertheless, when just looking at the radial errors over time, a strange behavior is obvious. In one 10-day segment, the radial errors are split in two groups. The first, in time, is at approximately −18 cm. The second group is at approximately +30 cm. Thus, this is for nearly ever 10-day segment the same, it seems that a systematic behavior is in the adjustment.

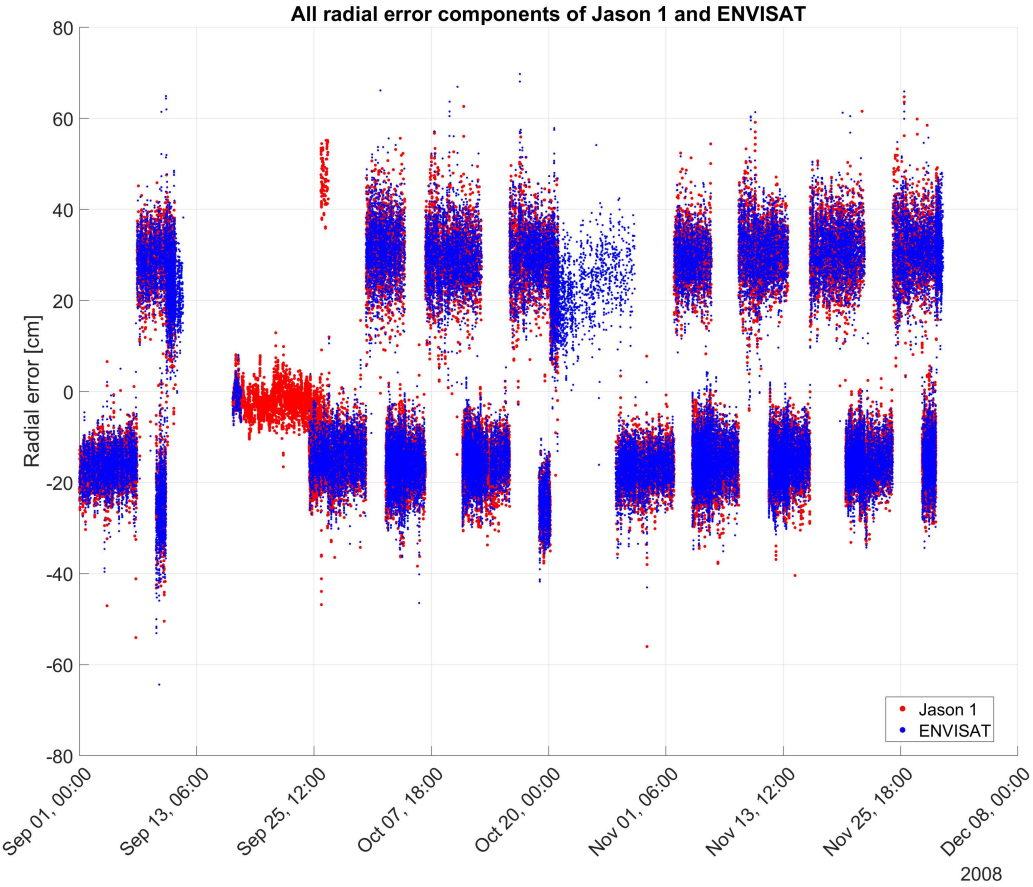

Figure 3.2: *All radial error components of Jason 1 and ENVISAT of the first time span over time.*

In the second time span wit Jason 2, 3 and SARAL/AltiKa the results look a bit different. As one can see in Figure 3.3 the radial errors are evenly distributed. Most of the radial errors seems to be in a range of -10 to +15 cm. Notice that the labeling of the color bar is different compared to Figure 3.1. Again, no geographically related patterns are visible. In both cases no correlation between the geography and the radial errors could be found. This leads to the conclusion that the geographic position of the radial errors has no influence.

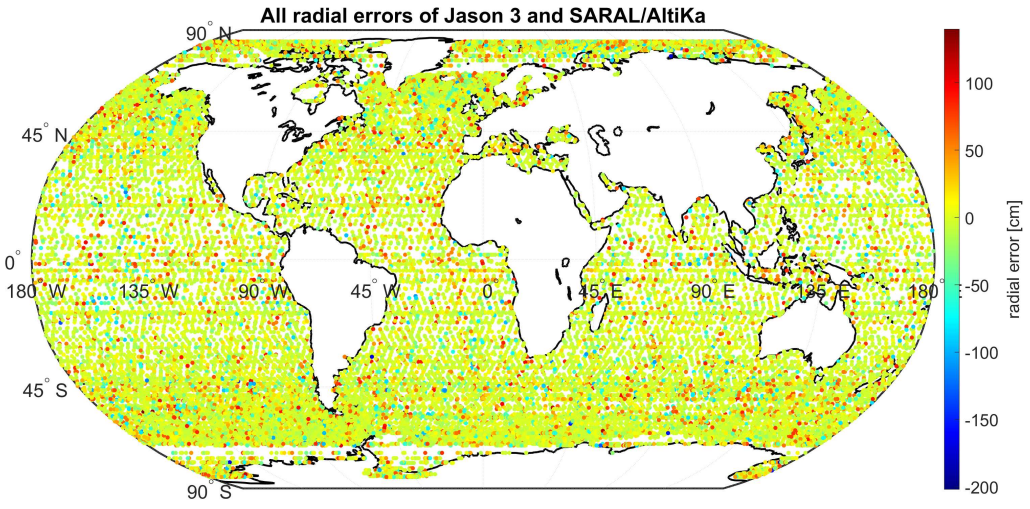

Figure 3.3: *All radial error components of Jason 3 and SARAL/AltiKa of the first time span, displayed on a world map.*

The errors over time are shown in Figure 3.4. An systematic behaviour is visible. One part of the 10-day segment contains errors in a range of ±20 cm. The second part has much larger radial errors. They are in range of ±100 cm.

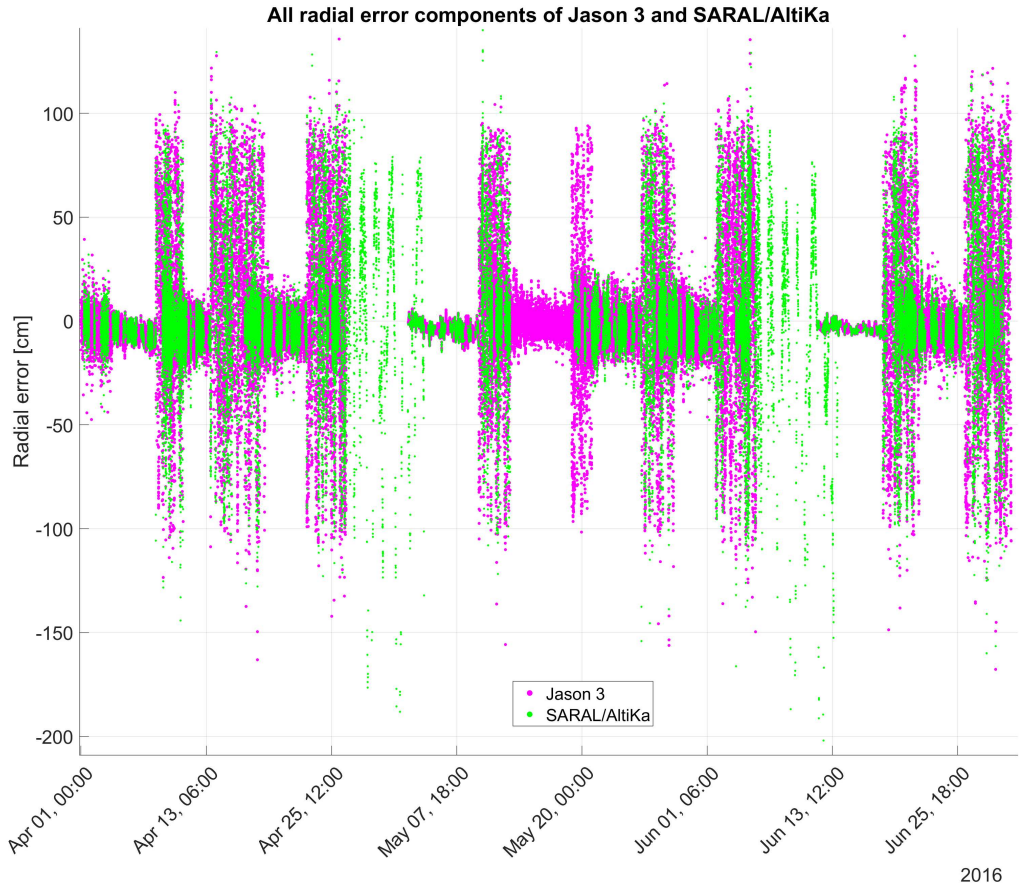

Figure 3.4: *All radial error components of Jason 3 and SARAL/AltiKa of the first time span over time.*

In both time periods, a systematic behaviour in the 10-day segments was found. The only explanation for this is, that this is caused during the adjustment of the crossover analysis. Nevertheless, the radial errors are used to reduce the bias.

Now, we have estimated the radial errors over the ocean. To apply them to inland altimetry, I selected the errors along the track passing over the site of interest (Figure 3.5). This is done for each pass of Lake Erie separately. For each crossover point, the satellite's altitude is known. As previously observed, geographical patterns are not found. Moreover, it is assumed that the magnitude of the radial error correlates with the satellite's altitude. Hence, a one-dimensional extrapolation of the radial errors based on altitude is conducted.

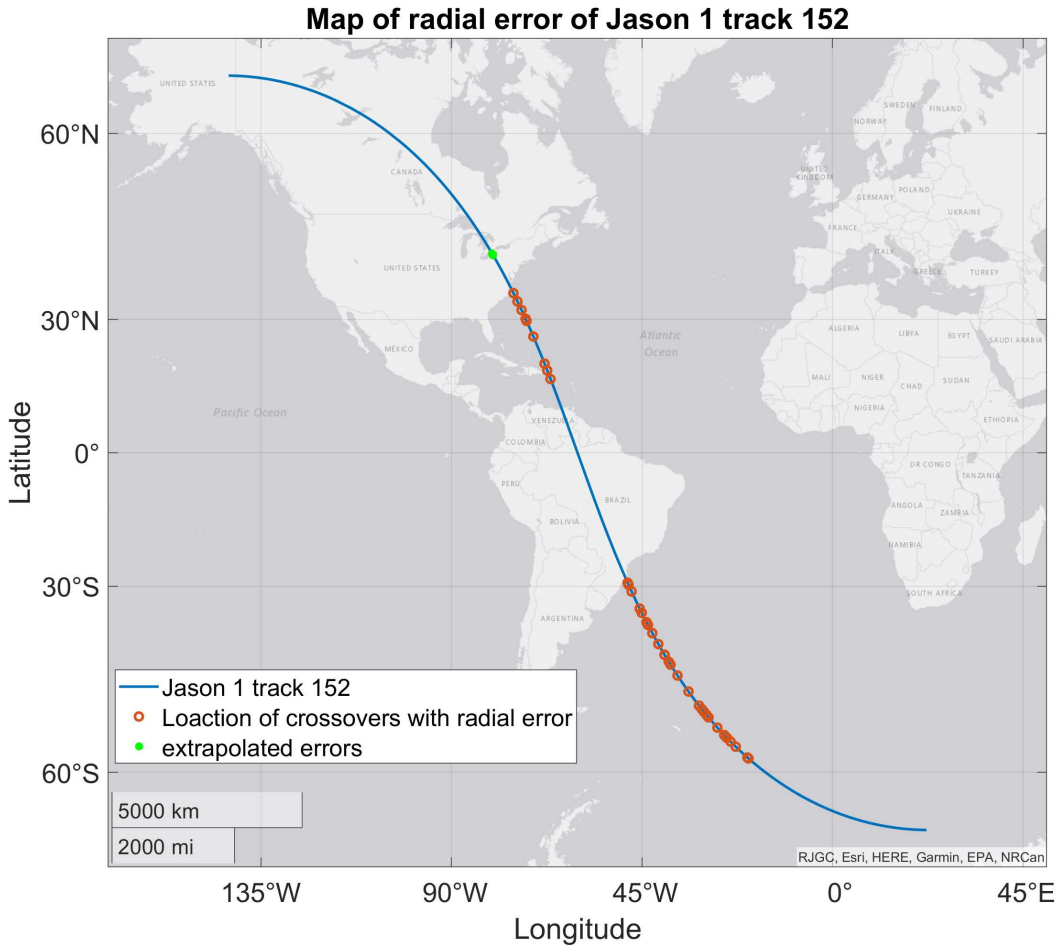

Figure 3.5: *Track 152 of Jason 1, with all used radial error components, in red, along track. The searched radial errors over Lake Erie are marked in green.*

Since, multiple different extrapolation methods existing, the extrapolation is performed with four different ones, in order to compare the different results. I chose the *linear*, shape-preserving piecewise cubic *pchip*, modified Akima cubic Hermite *makima* and *spline* methods, as they are the reasonable options in the *interp1* MATLAB function. pchip, makima and spline are all based on cubic polynomials (*1-D data interpolation (table lookup)*, n.d.).
After the extrapolation, the radial errors are added to the LLH values.

3.3 Results

First of all, the influence of different extrapolation methods is investigated. Therefor, only Jason 1 and Jason 2 is used. The results can be find in Table 3.1 and Figure 3.6.

Table 3.1: *Results of different extrapolation methods. The measurements come from track 152 from Jason 1 cycle 010 and Jason 2 cycle 249. The first row shows the results without any radial errors removed to the LLH.*

Mission	Solution	mean	median	Δmedian	std.
Jason 1	no errors	173.559 m	173.565 m	+5.1 cm	6.5 cm
Jason 2	removed	173.503 m	173.514 m		8.5 cm
Jason 1	linear extrap.	173.666 m	173.672 m	+3.8 cm	6.3 cm
Jason 2		173.620 m	173.634 m		8.8 cm
Jason 1	pchip extrap.	173.690 m	173.696 m	+2.4 cm	6.3 cm
Jason 2		173.657 m	173.672 m		8.8 cm
Jason 1	spline extrap.	175.154 m	175.148 m	+27.3 cm	8.9 cm
Jason 2		174.856 m	174.875 m		9.2 cm
Jason 1	makima extrap.	173.685 m	173.690 m	+3.2 cm	6.3 cm
Jason 2		173.644 m	173.658 m		8.8 cm

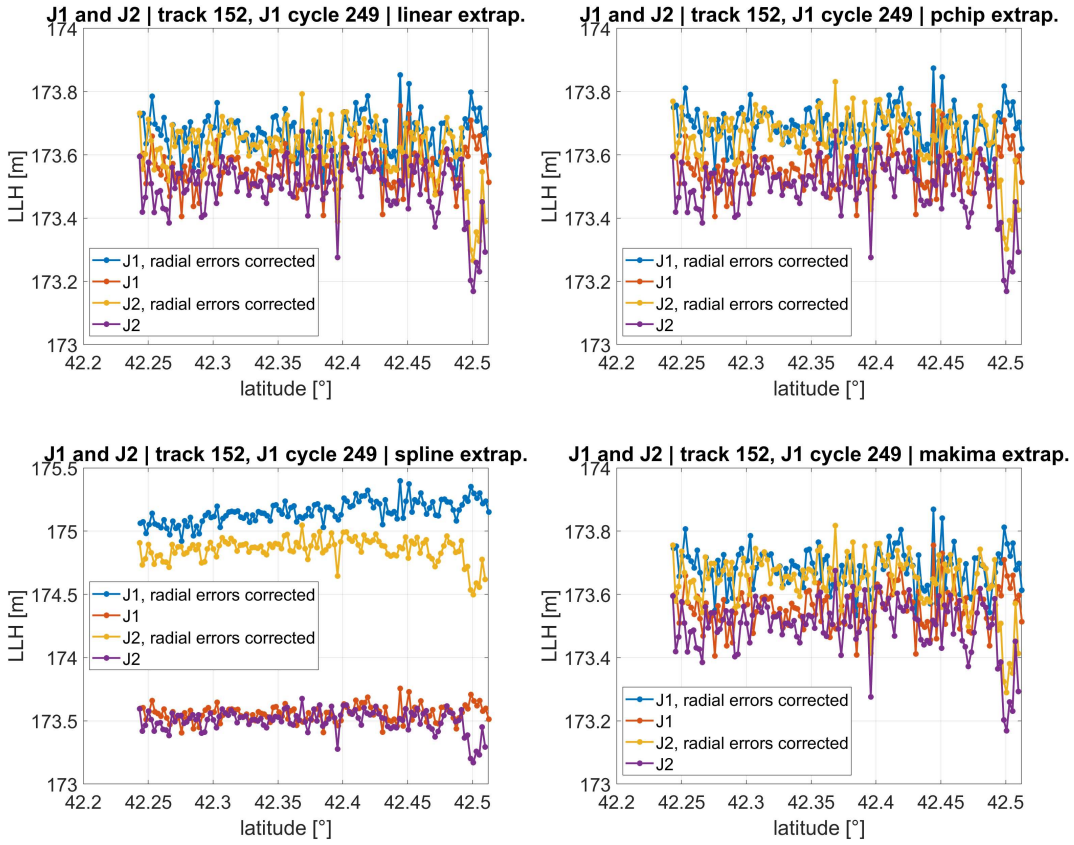

Figure 3.6: *The figure shows track 152 from Jason 1 cycle 010 and Jason 2 cycle 249 with radial errors removed. Each subplot shows the outcomes with different extrapolation methods*

When observing the differences in the medians (Δmedian), it is noticeable that attaching the radial errors reduced the bias, except for the spline solution, which worsened it. The best result is achieved with the pchip solution. The bias could be reduced to 2.4 cm.

When selecting the radial errors that are removed to the LLH, only those of Jason 1 and Jason 2, with themselves and each other, are used in the following Table 3.2.

Table 3.2: *Results of different extrapolation methods. The measurements come from track 152 from Jason 1 cycle 010 and Jason 2 cycle 249. The first row shows the results without any radial errors removed to the LLH.*

Mission	Solution	mean	median	Δmedian	std.
Jason 1	no errors	173.559 m	173.565 m	+5.1 cm	6.5 cm
Jason 2	removed	173.503 m	173.514 m		8.5 cm
Jason 1	linear extrap.	173.403 m	173.410 m	+1.0 cm	6.5 cm
Jason 2		173.390 m	173.400 m		8.6 cm
Jason 1	pchip extrap.	173.402 m	173.408 m	+0.2 cm	6.5 cm
Jason 2		173.396 m	173.406 m		8.6 cm
Jason 1	spline extrap.	173.028 m	173.034 m	-240.3 cm	6.7 cm
Jason 2		175.434 m	175.437 m		12.3 cm
Jason 1	makima extrap.	173.402 m	173.408 m	-50.2 cm	6.5 cm
Jason 2		173.896 m	173.910 m		8.6 cm

The Figure 3.7 shows the LLH values from which the results in Table 3.2 coming from.

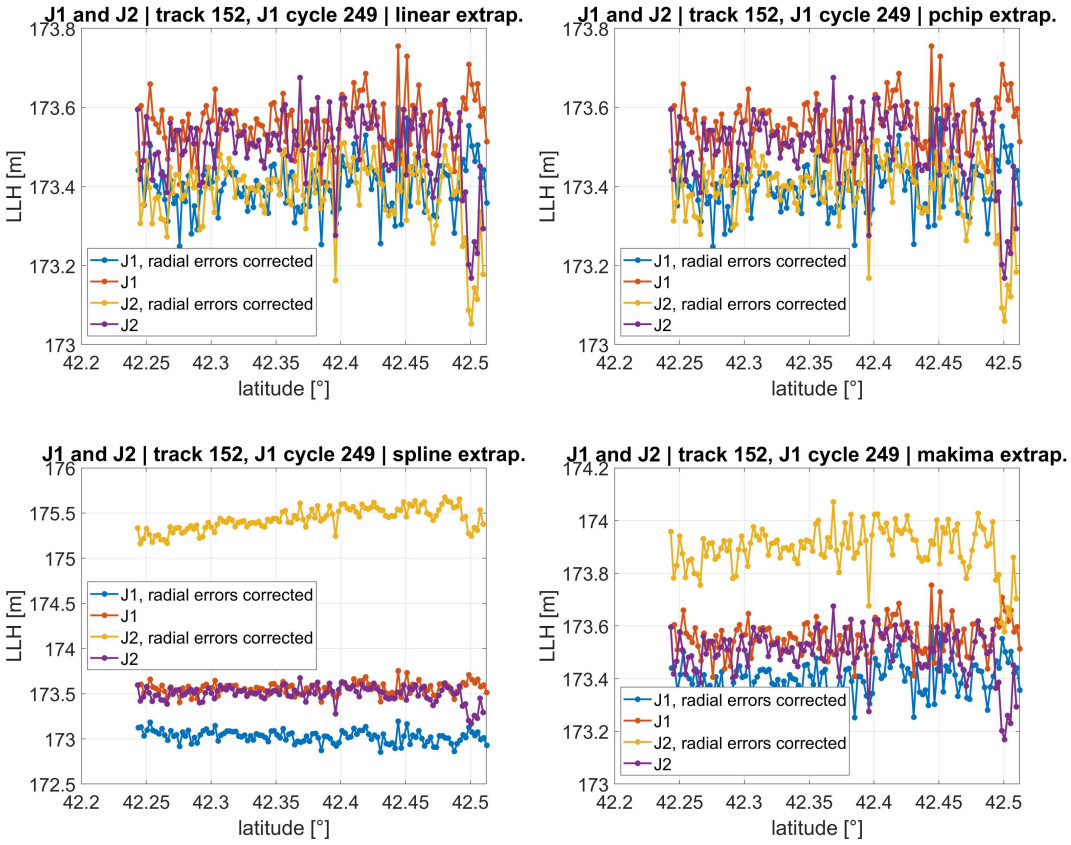

Figure 3.7: *The figure shows track 152 from Jason 1 cycle 010 and Jason 2 cycle 249 with radial errors removed. Each subplot shows the outcomes with different extrapolation methods*

The makima solution delivers bad results now, compared to the ones in Table 3.1. The spline solution is again very bad, with a difference of the medians of −240.3 cm. The linear and pchip solution reduced the difference by several centimeters. The smallest difference is with +0.2 cm at the pchip solution. For further investigations spline is no longer used, as the results were always really bad.
ENVISAT was operating during the time of the first set of radial errors. The results are shown in Figure 3.8.

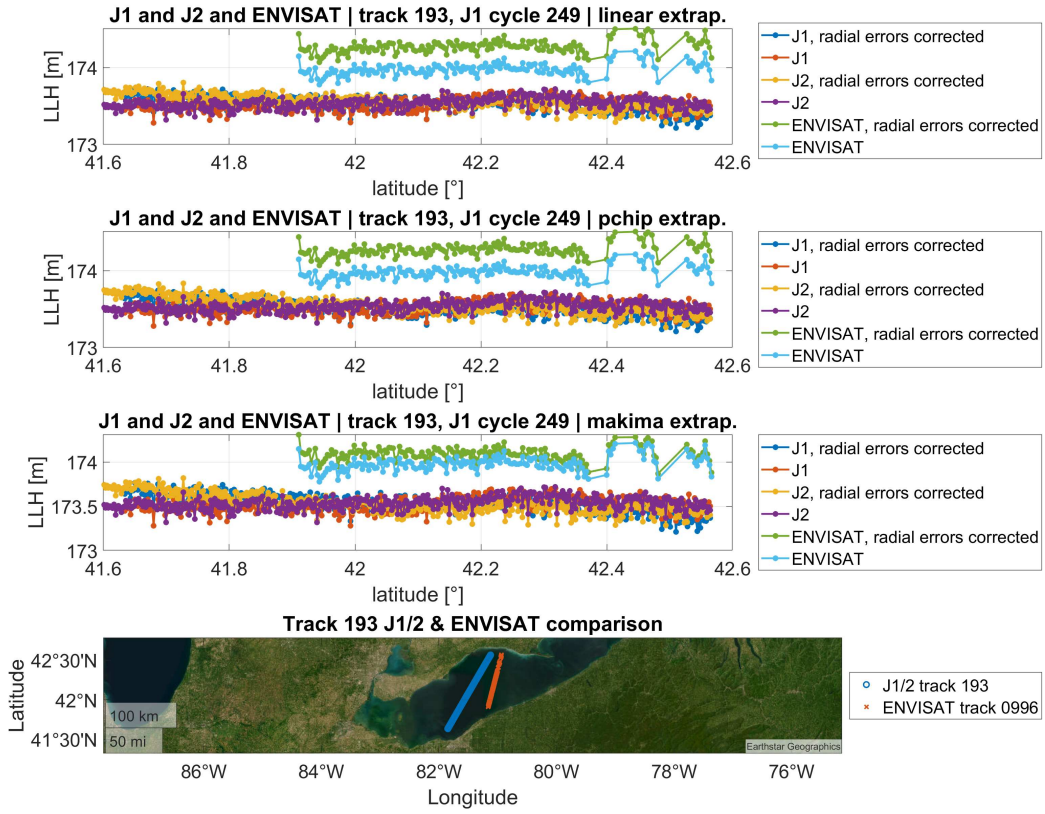

Figure 3.8: *The figure shows track 193 from Jason 1 cycle 010, Jason 2 cycle 249 and ENVISAT cycle 072 with radial errors removed. Each subplot shows the outcomes with linear, pchip and makima extrpolation methods*

In Table 3.3 the mean, median and standard deviation of the data shown in Figure 3.8 is shown. The difference between Jason 1 and Jason 2 increased after attaching the errors. After the attachment of the radial errors the difference between ENVISAT and the Jason satellites increased up to 72.3 cm. The smallest difference between Jason 1 and 2 is achieved with the linear method with −1.0 cm, which is an reduction of 0.7 cm.

Table 3.3: *Results of different extrapolation methods. The measurements come from track 152 from Jason 2 cycle 284, Jason 3 cycle 004 and ENVISAT cycle 032 track 0996. The first row shows the results without any radial errors removed to the LLH. At the column* **Δmedian** *the differences are always formed in the following order: Jason 1 - Jason 2; Jason 1 - ENVISAT; Jason 2 - ENVISAT*

Mission	Solution	mean	median	Δmedian	std.
Jason 1	no errors removed	173.521 m	173.521 m	-1.7 cm	7.4 cm
Jason 2		173.535 m	173.538 m	-46.1 cm	6.9 cm
ENVISAT		173.981 m	173.982 m	-44.4 cm	8.2 cm
Jason 1	linear extrap.	173.531 m	173.543 m	-1.0 cm	9.5 cm
Jason 2		173.553 m	173.553 m	-73.3 cm	9.5 cm
ENVISAT		174.275 m	174.276 m	-72.3 cm	8.2 cm
Jason 1	pchip extrap.	173.514 m	173.514 m	-1.9 cm	10.2 cm
Jason 2		173.544 m	173.533 m	-76.0 cm	11.1 cm
ENVISAT		174.273 m	174.274 m	-74.1 cm	8.2 cm
Jason 1	makima extrap.	173.536 m	173.542 m	+3.2 cm	10.3 cm
Jason 2		173.528 m	173.510 m	-55.2 cm	10.7 cm
ENVISAT		174.090 m	174.094 m	-58.4 cm	7.5 cm

ENVISAT does clearly not match with Jason 1 and Jason 2. It must be mentioned that ENVISAT flies not over the same area of Lake Erie. ENVISAT also flies over Lake Erie approximately 2 days after Jason 1 and Jason 2. Nevertheless, the difference is too great to be explained by this. Why the difference increased is unknown.

The second set of radial errors covers all crossovers from April 1, 2016 to July 1, 2016. All radial errors during that time span are used for the following results. The SSH was computed with MLE3 for Jason 2 and Jason 3. This time span covers the tandem phase of Jason 2 and 3. SARAL/AltiKa worked at the same time. The results can be seen in Figure 3.9.

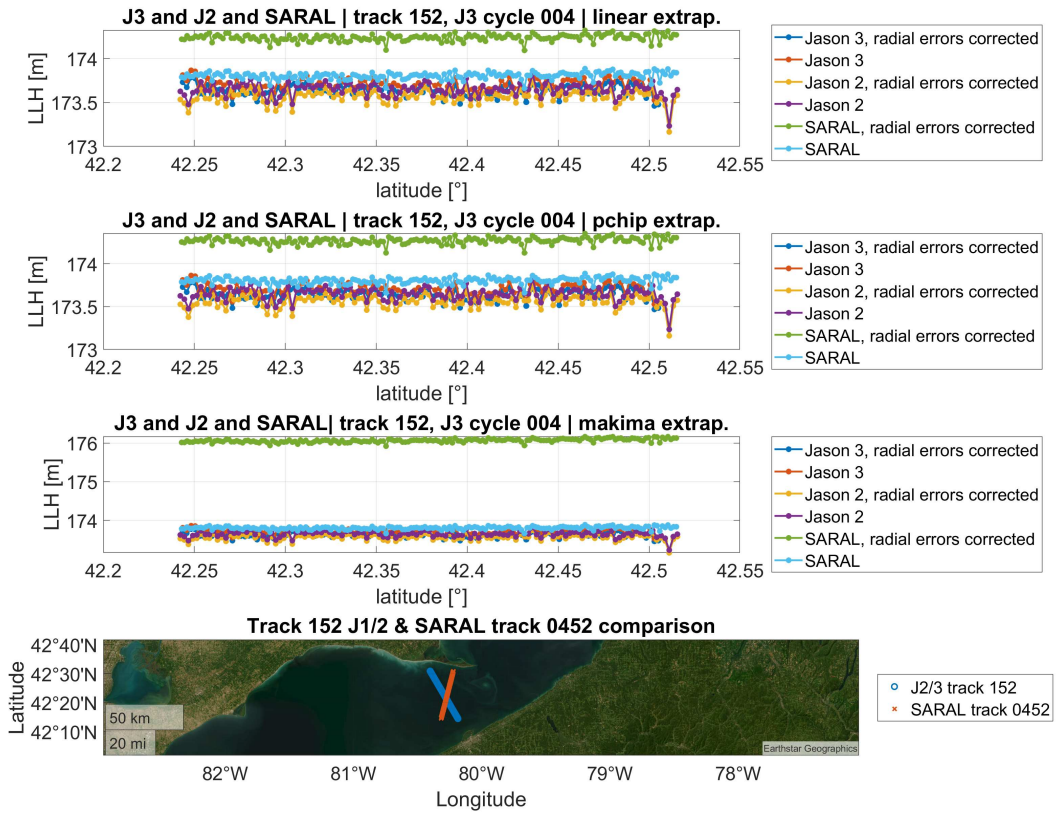

Figure 3.9: *The figure shows track 152 from Jason 2 cycle 284 Jason 3 cycle 004 and SARAL/AltiKa cycle 032 with radial errors removed. Each subplot shows the outcomes with linear, pchip and makima extrpolation methods*

SARAL/AltiKa has a visible difference to Jason 2 and 3. With removed radial errors the difference is still there. It is obvious that the makima extrapolation method did not work very well as the difference growth over a meter.

Table 3.4: *Results of different extrapolation methods. The measurements come from track 152 from Jason 2 cycle 284, Jason 3 cycle 004 and SARAL/AltiKa cycle 032 track 0452. The first row shows the results without any radial errors removed to the LLH. At the column* ***Δmedian*** *the differences are always formed in the following order: Jason 3 - Jason 2; Jason 3 - SARAL/AltiKa; Jason 2 - SARAL/AltiKa*

Mission	Solution	mean	median	Δmedian	std.
Jason 3	no errors removed	173.705m	173.708m	5.8 cm	6.6 cm
Jason 2		173.645 m	173.650 m	-10.0 cm	7.7 cm
SARAL/AltiKa		173.805 m	173.808 m	-15.8 cm	3.7 cm
Jason 3	linear extrap.	173.633 m	173.632 m	5.7 cm	6.6 cm
Jason 2		173.564 m	173.575 m	-60.9 cm	7.6 cm
SARAL/AltiKa		174.239 m	174.241 m	-66.6 cm	3.7 cm
Jason 3	pchip extrap.	173.635 m	173.634 m	6.4 cm	6.6 cm
Jason 2		173.559 m	173.570 m	-63.9 cm	7.6 cm
SARAL/AltiKa		174.270 m	174.273 m	-70.3 cm	3.7 cm
Jason 3	makima extrap.	173.630 m	173.629 m	5.2 cm	6.6 cm
Jason 2		173.565 m	173.577 m	-243.9 cm	7.6 cm
SARAL/AltiKa		176.064 m	176.068 m	-249.1 cm	4.5 cm

From the results in the Table 3.4 it can be seen that removing the radial errors components, reduces the differences between Jason 2 and Jason 3 with the linear and makima solution. The best reduction, from 5.8 cm to 5.2 cm, is achieved with the makima function. On the other hand the differences with SARAL/AltiKa became larger by up to −249.9 cm with the makima solution. Why it worked out for Jason 2 and 3 but not for SARAL/AltiKa could not be found out.
Here it has to be mentioned as well, that there is a time difference of approx. 6 days between Jason 2, 3 and SARAL/AltiKa.
Overall one can say that the radial error estimation worked well for the Jason satellites. Other missions as ENVISAT or SARAL/AltiKa did not benefit from it.

Chapter 4

Bias analysis

4.1 Time series during tandem phase of Jason satellites

As mentioned (Section 1.2.1) the Jason satellites are passing on the same orbit with approximately one minute difference. Thus, it it possible to compare the measurements during that phase. In the nominal Jason orbit, there are three passes (tracks) over Lake Erie. Track 76 and 152 are descending and track 193 is ascending (Figure 1.5).
In the following the differences between the satellites and retracking algorithms are shown at selected cycles, to demonstrate the problem between different satellite missions. The plots are showing the lake level height (LLH) of Lake Erie and the location of the measurements. The LLH includes all atmospheric and tidal corrections for inland altimetry. These are the dry and wet troposphere, ionosphere, pole tide and solid earth tide. The mean sea surface is also attached. The Table 4.1 shows which atmospheric corrections are used for each mission. The wet troposphere corrections from the radiometers are used over the open waters of Lake Erie, but not in the coastal regions. The ECMWF model corrections are only applied where no radiometer corrections are available.

Table 4.1: *The table lists the wet and dry troposheric corrections, as well as the ionospheric correction that are used, unless otherwise is noted; ECMWF: European Center for Medium Range Weather Forecasting; JMR: Jason Microwave Radiometer; AMR: Advanced Microwave Radiometer; MWR: Microwave Radiometer*

Mission	Wet Troposphere	Dry Troposphere	Ionosphere
Jason 1	JMR & model (ECMWF)	model (ECMWF)	dual-frequation
Jason 2	AMR & model (ECMWF)	model (ECMWF)	dual-frequation
Jason 3	AMR & model (ECMWF)	model (ECMWF)	dual-frequation
ENVISAT	MWR & model (ECMWF)	model (ECMWF)	GIM (from GDR)
SARAL	AMR & model (ECMWF)	model (ECMWF)	GIM (from GDR)

The satellites have different reference ellipsoids in the used GDR (Geophysical Data Record) products. If they are different to the WGS84, they are changed. This is achieved

by calculating the difference between the current reference ellipsoid and the WGS84 ellipsoid. This difference will be added to the provided altitude.
The mean sea surfaces from the GDR products are not used. Instead, the geoid height is taken from the MATLAB internal function *geoidheight*, which uses the EGM2008 geopotential model (*Calculate geoid height*, n.d.).
The following plots are randomly chosen examples of passes over Lake Erie, during the tandem phases of the Jason satellites. Jason 1 has only MLE4, Jason 2 and 3 have MLE3 and MLE4 retracking.

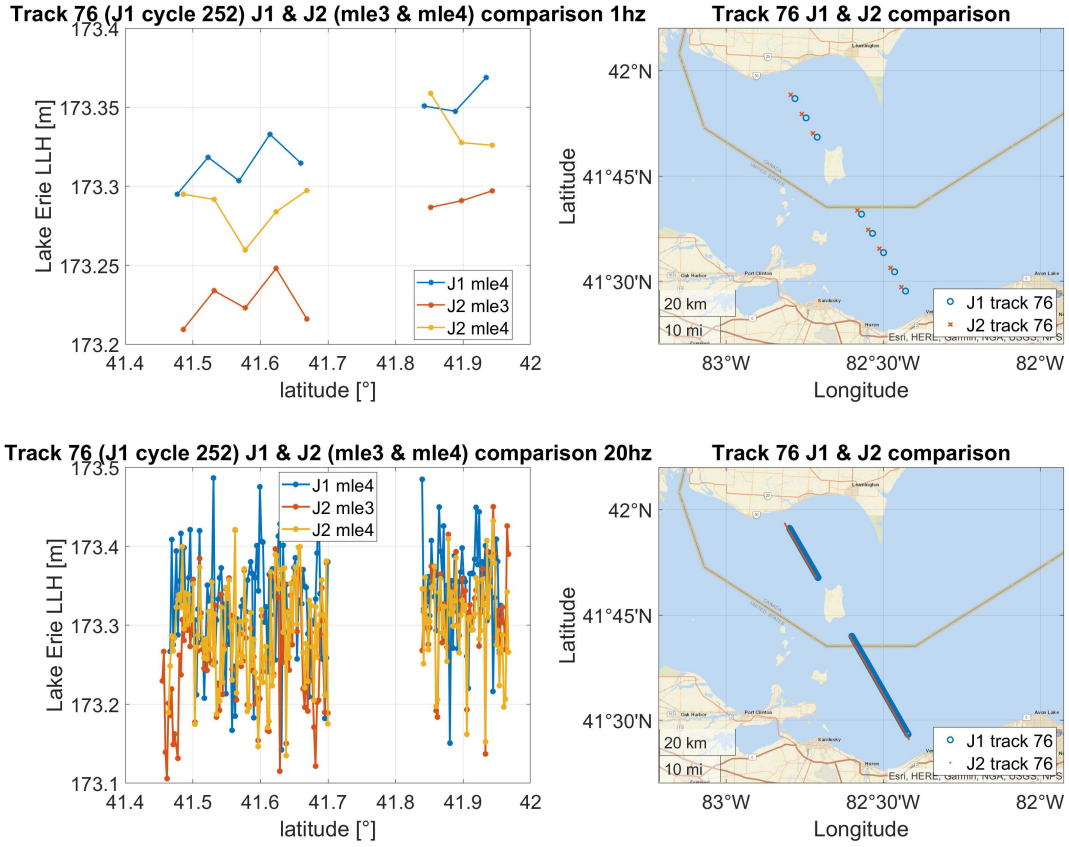

Figure 4.1: *Lake Erie LLH, Track 76 from Jason 1 cycle 252, Jason 2 cycle 013. On the top left are the reduced 1 Hz measurements, on the bottom left are the 20 Hz measurements. On the corresponding right side are maps that are showing the locations where the measurements are taken.*

Because track 76 goes over an island, the track is divided in two parts. This is visible in the Figure 4.1, 4.4, 4.18. In Figure 4.1 it is clearly visible, in the 1 Hz and 20 Hz data, that Jason 1 tend to measure a higher LLH than Jason 2. In the reduced 1 Hz measurements, the difference between Jason 2 using MLE3 and MLE4 retracking is several centimeters. In comparison to the 20 Hz data, there is nearly no difference visible. This is also visible in Figure 4.2.
In contrast to the figure above (Figure 4.1), in Figure 4.2 Jason 1 tend to measure a lower

LLH values than Jason 1. The difference here between the two retracking algorithms of Jason 2 is smaller, although the difference in 20 Hz data seems to be smaller again compared to the reduced 1 Hz data.
For track 193 the differences are not as big as in track 76 or 152, which can be seen when comparing Figure 4.3 with Figure 4.1 or Figure 4.2.

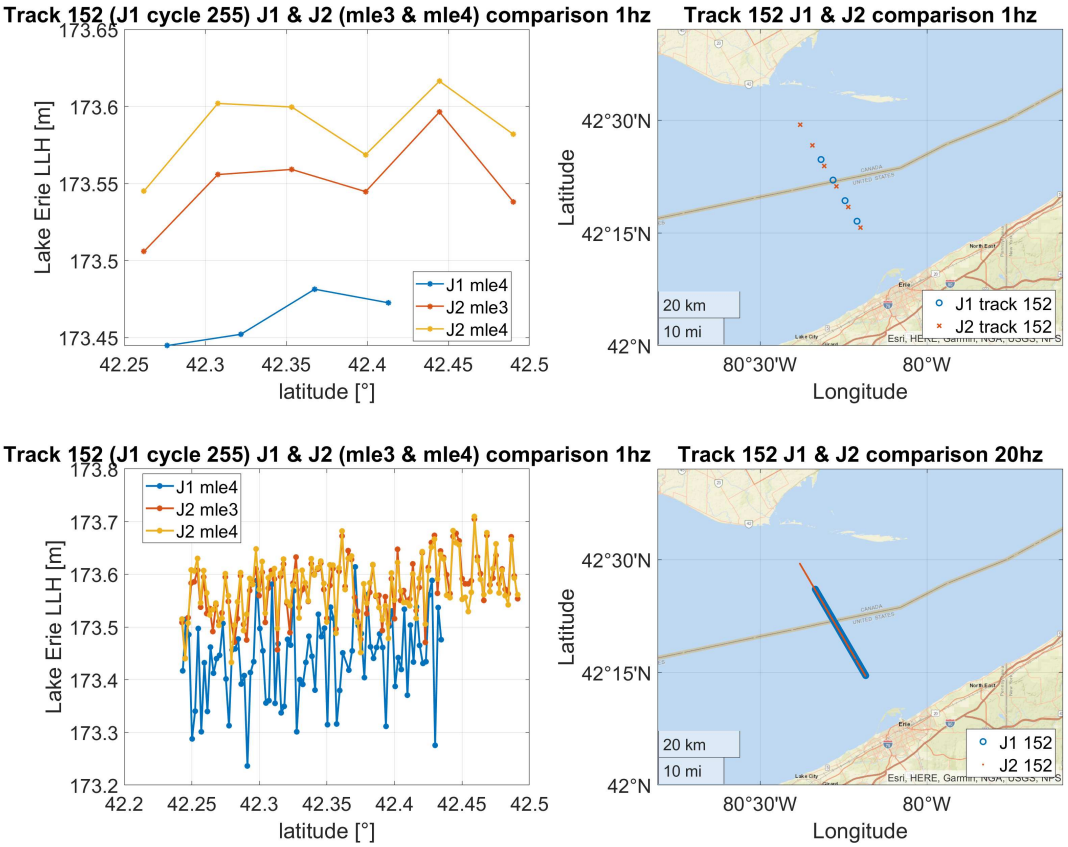

Figure 4.2: *Lake Erie LLH, Track 152 from Jason 1 cycle 255, Jason 2 cycle 016. On the top left are the reduced 1 Hz measurements, on the bottom left are the 20 Hz measurements. On the corresponding right side are maps that are showing the locations where the measurements are taken.*

In the following, the values in the tables are being analyzed. Differences mentioned are always between the median values, unless otherwise is mentioned.
The Table 4.2 lists the mean, median and standard deviation (std) of the 1 Hz data, that is shown in the Figures 4.1, 4.2 and 4.3. The smallest difference between Jason 1 and Jason 2 is at the tracks 76 and 193. At track 76 the difference between Jason 1 MLE4 and Jason 2 MLE4 is −3.0 cm. At track 193 the difference between Jason 1 MLE4 and Jason 2 MLE3 is 3.0 cm. The largest difference is at track 152 between Jason 1 MLE4 and Jason 2 MLE4 with 12.9 cm. There are also differences at Jason 2 between the two retracking algorithms. The smallest one is at track 193 with 1.4 cm and the biggest one is at track 76 with 5.5 cm.

Table 4.2: *Mean, median and standard deviation (std) of 1 Hz measurements, which are visualized in Figure 4.1, 4.2 and 4.3. At the column* ***Δmedian*** *the differences are always formed in the following order: Jason 1 - Jason 2 MLE4; Jason 1 - Jason 2 MLE3; Jason 2 MLE4 - Jason 2 MLE3. Acronyms: Jason 1 (J1), Jason 2 (J2), track (t.), cycle (c.)*

1 Hz	mean	median	std.	Δmedian
J1, MLE4, t.76, c.252	173.329 m	173.326 m	2.5 cm	+3.0 cm
J2, MLE4, t.76, c.013	173.305 m	173.296 m	3.1 cm	+8.5 cm
J2, MLE3, t.76, c.013	173.251 m	173.241 m	3.6 cm	+5.5 cm
J1, MLE4, t.152, c.255	173.463 m	173.462 m	1.7 cm	-12.9 cm
J2, MLE4, t.152, c.016	173.586 m	173.591 m	2.6 cm	-8.8 cm
J2, MLE3, t.152, c.016	173.550 m	173.550 m	3.0 cm	+4.1 cm
J1, MLE4, t.193, c.249	173.513 m	173.504 m	3.1 cm	-4.4 cm
J2, MLE4, t.193, c.010	173.552 m	173.548 m	3.2 cm	-3.0 cm
J2, MLE3, t.193, c.010	173.543 m	173.534 m	3.6 cm	+1.4 cm

The Table 4.3 is showing the mean, median and standard deviation (std) of the 20 Hz measurements that are shown in the Figure 4.1, 4.2 and 4.3. At track 152, the difference between Jason 1 MLE4 and Jason 2 MLE4 is the largest one with −13.1 cm. The smallest difference is at track 193, between Jason 1 MLE4 and Jason 2 MLE4, with −1.7 cm. At Jason 2 the difference between MLE3 and MLE4 is varying between 0.1 cm and 1.0 cm.

Table 4.3: *Mean, median and standard deviation (std) of 20 Hz measurements, which are visualized in Figure 4.1, 4.2 and 4.3. At the column* ***Δmedian*** *the differences are always formed in the following order: Jason 1 - Jason 2 MLE4; Jason 1 - Jason 2 MLE3; Jason 2 MLE4 - Jason 2 MLE3. Acronyms: Jason 1 (J1), Jason 2 (J2), track (t.), cycle (c.)*

20 Hz	mean	median	std.	Δmedian
J1, MLE4, t.76, c.252	173.332 m	173.335 m	6.6 cm	+3.4 cm
J2, MLE4, t.76, c.013	173.295 m	173.301 m	6.2 cm	+4.4 cm
J2, MLE3, t.76, c.013	173.283 m	173.291 m	7.2 cm	+1.0 cm
J1, MLE4, t.152, c.255	173.441 m	173.449 m	8.0 cm	-13.1 cm
J2, MLE4, t.152, c.016	173.576 m	173.580 m	5.4 cm	-13.0 cm
J2, MLE3, t.152, c.016	173.575 m	173.579 m	5.4 cm	+0.1 cm
J1, MLE4, t.193, c.249	173.520 m	173.519 m	7.3 cm	-2.5 cm
J2, MLE4, t.193, c.010	173.541 m	173.544 m	6.8 cm	-1.7 cm
J2, MLE3, t.193, c.010	173.534 m	173.536 m	6.7 cm	+0.8 cm

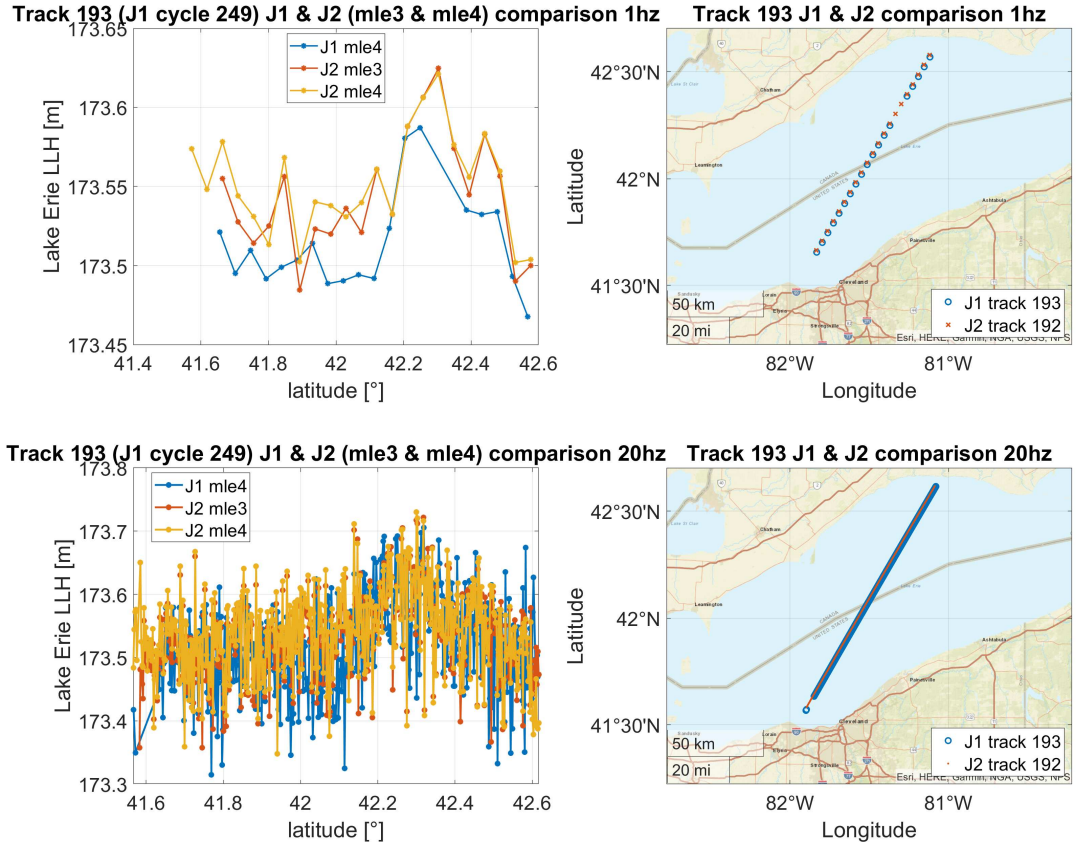

Figure 4.3: *Lake Erie LLH, Track 193 from Jason 1 cycle 249, Jason 2 cycle 010. On the top left are the reduced 1 Hz measurements, on the bottom left are the 20 Hz measurements. On the corresponding right side are maps that are showing the locations where the measurements are taken.*

The Figure 4.4, 4.5 and 4.6 are comparing Jason 2 with Jason 3 during their tandem phase. Jason 2 and 3 are both provided with the MLE3 and MLE4 retracking algorithms (*OSTM/Jason-2 Products Handbook*, 2017)(*Jason-3 Products Handbook*, 2021). In Figure 4.4 the gap due to the island is visible. For all three tracks that are viewed, Jason 2 and Jason 3 have always observed a different LLH.

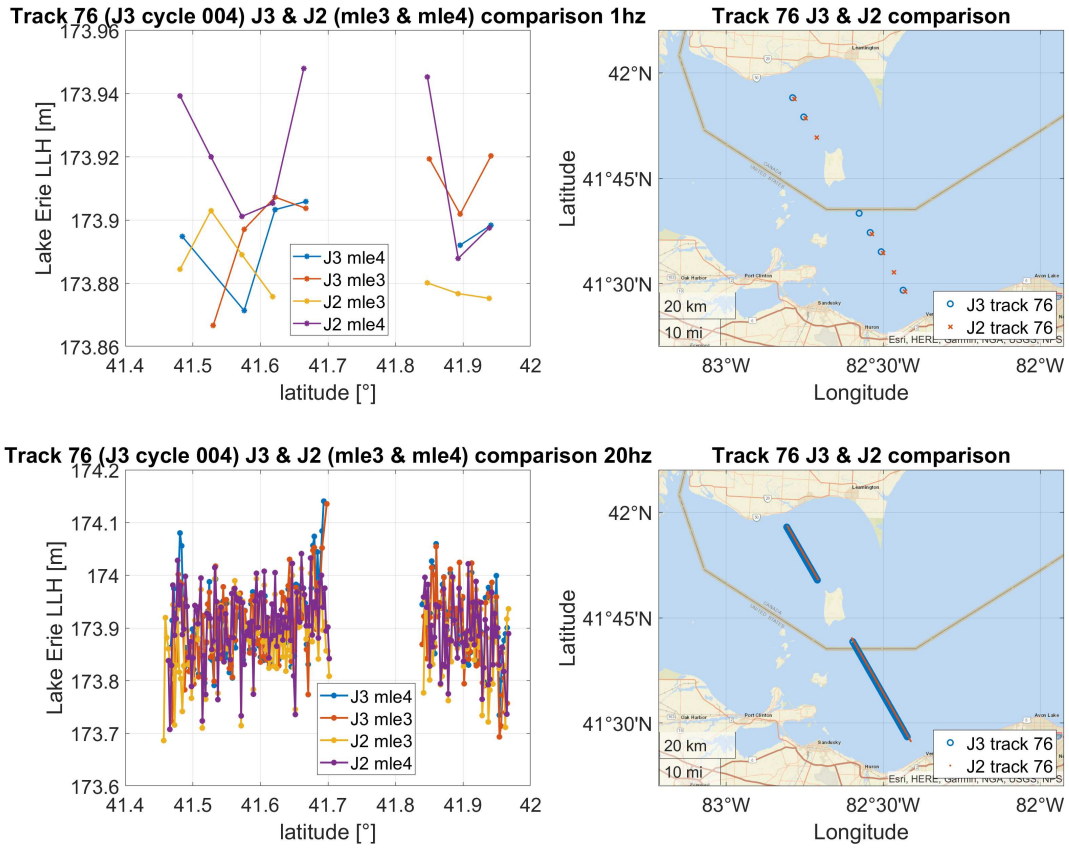

Figure 4.4: *Lake Erie LLH, Track 76 from Jason 2 cycle 284, Jason 3 cycle 004. On the top left are the reduced 1 Hz measurements, on the bottom left are the 20 Hz measurements. On the corresponding right side are maps that are showing the locations where the measurements are taken.*

In Figure 4.5 one can see that the MLE3 and MLE4 solution for Jason 2 are quite different from each other. A noticeable difference exist for both, 1 Hz and 20 Hz measurements. In comparison to the results from Jason 1 and 2, Jason 2 has no such big difference between MLE3 and MLE4.

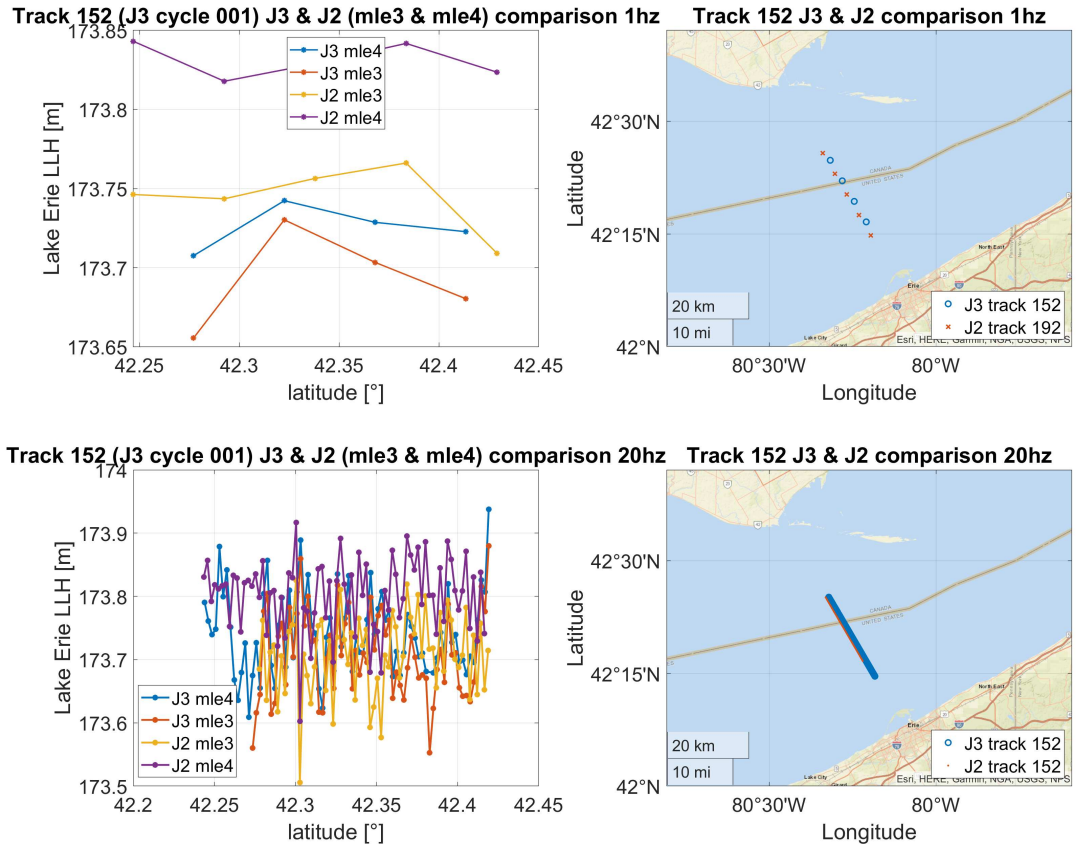

Figure 4.5: *Lake Erie LLH, Track 152 from Jason 1 cycle 281, Jason 2 cycle 001. On the top left are the reduced 1 Hz measurements, on the bottom left are the 20 Hz measurements. On the corresponding right side are maps that are showing the locations where the measurements are taken.*

The Table 4.4 lists the mean, median and standard deviation (std) of the 1 Hz data, that are shown in the Figures 4.4, 4.5 and 4.6. All differences refer to Jason 3 MLE4, as it serves as a reference mission. The smallest difference between Jason 2 and the reference is with Jason 2 MLE3 at the track 76 with 0.9 cm. The largest difference is at Jason 2 MLE4, track 152 with 13.7 cm. There are also differences between the two retracking algorithms at each satellite. For Jason 3 the smallest one is at track 193 with 0.3 cm. The largest one is at track 152 with 3.4 cm. For Jason 2 the smallest difference is at track 193 with 0.5 cm and the largest one is at track 152 with 8.3 cm.

Table 4.4: *Mean, median and standard deviation (std) of 1 Hz measurements, which are visualized in Figure 4.4, 4.5 and 4.6. Jason 3 MLE4 serves as the reference mission for the differences. Acronyms: Jason 3 (J3), Jason 2 (J2), track (t.), cycle (c.)*

1 Hz	mean	median	std.	Δmedian
J3, MLE4, t.76, c.004	173.894 m	173.904 m	1.2 cm	-
J3, MLE3, t.76, c.004	173.902 m	173.897 m	1.8 cm	-0.7 cm
J2, MLE4, t.76, c.284	173.918 m	173.913 m	2.4 cm	-2.4 cm
J2, MLE3, t.76, c.284	173.884 m	173.880 m	1.0 cm	+0.9 cm
J3, MLE4, t.152, c.001	173.725 m	173.692 m	1.4 cm	-
J3, MLE3, t.152, c.001	173.692 m	173.726 m	3.2 cm	+3.4 cm
J2, MLE4, t.152, c.281	173.831 m	173.829 m	1.1 cm	+13.7 cm
J2, MLE3, t.152, c.281	173.744 m	173.746 m	2.2 cm	+5.4 cm
J3, MLE4, t.193, c.008	174.213 m	174.209 m	6.0 cm	-
J3, MLE3, t.193, c.008	174.209 m	174.211 m	6.0 cm	+0.2 cm
J2, MLE4, t.193, c.288	174.196 m	174.193 m	5.2 cm	-1.6 cm
J2, MLE3, t.193, c.288	174.194 m	174.188 m	5.2 cm	-2.1 cm

The Table 4.5 is showing the mean, median and standard deviation (std) of the 20 Hz measurements that are shown in the Figures 4.4, 4.5 and 4.6. The smallest difference between Jason 2 and the reference is at track 76, with 0.4 cm. the largest one is at track 152 with 10.3 cm. The difference between the two retracking algorithms of one satellite, is smallest at track 193 Jason 2, with 0.2 cm. The largest is at track 152 Jason 2, with 9.7 cm.

Table 4.5: *Mean, median and standard deviation (std) of 20 Hz measurements, which are visualized in Figure 4.4, 4.5 and 4.6. Jason 3 MLE4 serves as the reference mission for the differences. Acronyms: Jason 3 (J3), Jason 2 (J2), track (t.), cycle (c.)*

20 Hz	mean	median	std.	Δmedian
J3, MLE4, t.76, c.004	173.912 m	173.902 m	6.9 cm	-
J3, MLE3, t.76, c.004	173.901 m	173.910 m	7.5 cm	+0.8 cm
J2, MLE4, t.76, c.284	173.902 m	173.886 m	6.7 cm	-1.6 cm
J2, MLE3, t.76, c.284	173.879 m	173.906 m	6.8 cm	+0.4 cm
J3, MLE4, t.152, c.001	173.743 m	173.706 m	6.5 cm	-
J3, MLE3, t.152, c.001	173.708 m	173.739 m	6.9 cm	+3.3 cm
J2, MLE4, t.152, c.281	173.802 m	173.809 m	5.7 cm	+10.3 cm
J2, MLE3, t.152, c.281	173.708 m	173.712 m	6.4 cm	+0.6 cm
J3, MLE4, t.193, c.008	174.207 m	174.205 m	8.5 cm	-
J3, MLE3, t.193, c.008	174.206 m	174.208 m	8.5 cm	+0.3 cm
J2, MLE4, t.193, c.288	174.185 m	174.182 m	7.5 cm	-2.3 cm
J2, MLE3, t.193, c.288	174.182 m	174.180 m	7.4 cm	-2.5 cm

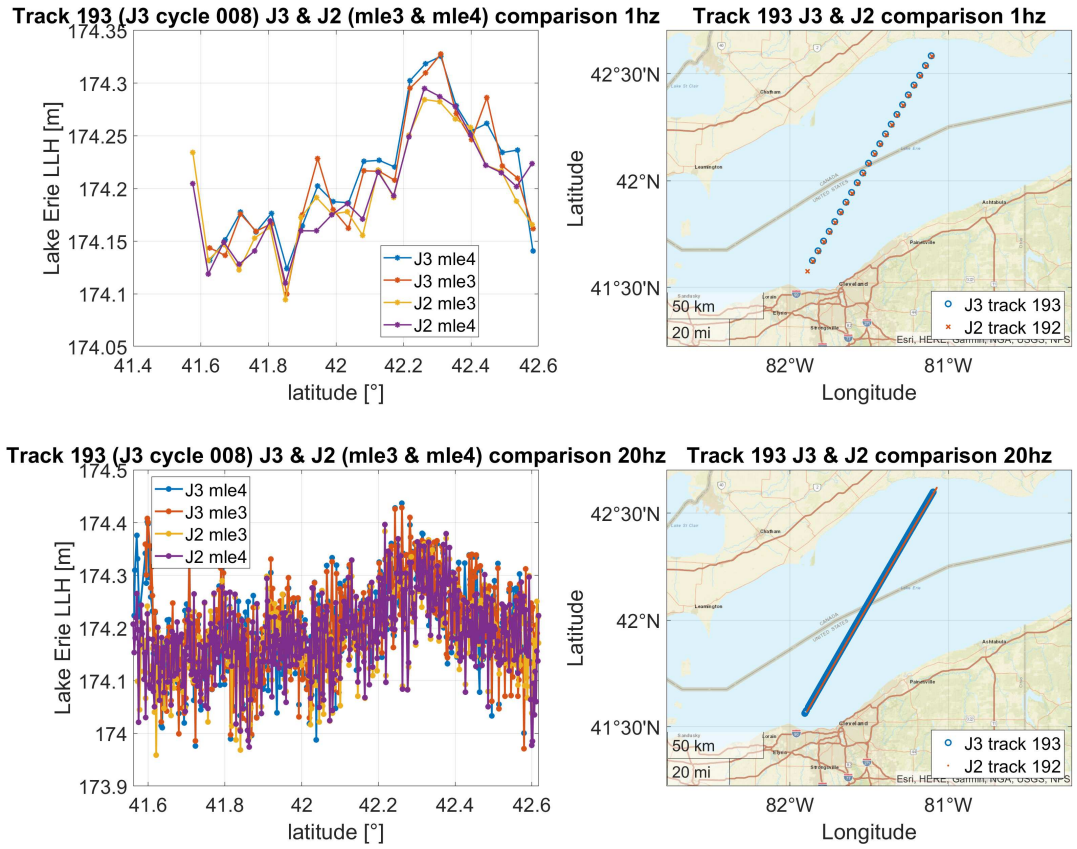

Figure 4.6: *Lake Erie LLH, Track 193 from Jason 1 cycle 288, Jason 2 cycle 008. On the top left are the reduced 1 Hz measurements, on the bottom left are the 20 Hz measurements. On the corresponding right side are maps that are showing the locations where the measurements are taken.*

On the whole, differences of several centimeters between satellites and their respective retracking algorithms can arise. The next two sections (Section 4.1.2 and Section 4.1.1) explore two distinct approaches to minimize these differences. Section 4.1.2 examines the impact of distinct corrections provided individually for each satellite, while Section 4.1.1 focuses on observing the influence of retracking algorithms on the measurements.

4.1.1 Retracking investigations

In this section we will have a closer look at the retracking algorithms. As in Section 4.1 the tandem phases of the Jason series are used to provide a comparison under the same circumstances. Jason 1 is provided with the MLE4 retracking algorithm. Jason 2 and 3 are provided with the MLE4 and MLE3 algorithm.

Determining all retracking bins of one overflight over Lake Erie, during the tandem phase, allows a comparison between the satellites and their retracking algorithms. In Figure 4.7 the radargram of track 193 of Jason 1 cycle 249 and Jason 2 cycle 010 are shown. It is visible that the retracking bins of Jason 1 tend to be lower than the retracking bins of Jason 2. The differences of MLE3 and MLE4 retracking for Jason 2 are quite small.
The same bins are also visualized in Figure 4.8 for a better visual comparability. In the Table 4.6 the mean, median and standard deviation (std) of the retracking bins are listed. Comparing Jason 1 and Jason 2, the maximal difference for the mean is 0.446 bins, between Jason 1 MLE4 and Jason 2 MLE4. At the median the MLE3 and MLE4 retracking are the same for Jason 2. The difference there between Jason 1 and Jason 2 is 0.453 bins. The standard deviations are also quit similar. Between Jason 2 MLE3 and MLE4 it is just 0.01 bins difference. The standard deviation of Jason 1 is with 0.280 a little bit smaller, which leads to 0.08 (MLE3) and 0.09 bins (MLE4) differences.
As the differences of the mean and median are both bigger than the standard deviations, it seems possible that a bias could accrue due to retracking. To proof if this is really the case further investigations have to be done.

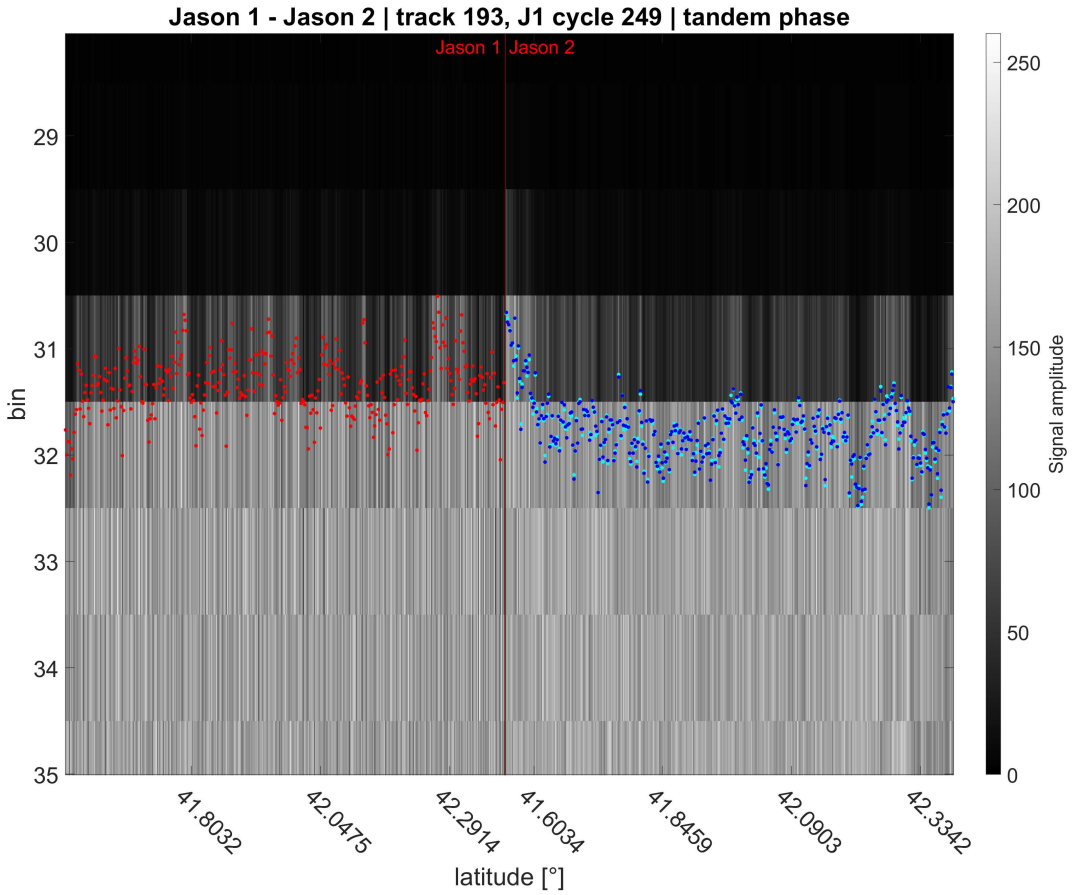

Figure 4.7: *The figure is showing cutouts of the waveforms reflected from Lake Erie, during the tandem phase of Jason 1 and Jason 2. It shows cutouts of one overflight over Lake Erie (track 193). The brightness symbolises the signal amplitude. The graphic is divided by the red line. On left are the waves of Jason 1, on the right are the waves from Jason 2. The x-axis shows the total number of waves. The red points are the retracked points of Jason 1 with MLE4 algorithm. The blue and cyan ones are the retracking points, MLE3 and MLE4, of Jason 2.*

Table 4.6: *The table is showing the mean, median and the standard deviation (std) of the retracking bins of track 193 from Jason 1 cycle 249 and Jason 2 cycle 010. The bins are also visualized in the Figure 4.7 and 4.8*

	mean [bin]	median [bin]	std [bin]
Jason 1 MLE4	31.335	31.334	0.280
Jason 2 MLE4	31.781	31.787	0.289
Jason 2 MLE3	31.776	31.787	0.288

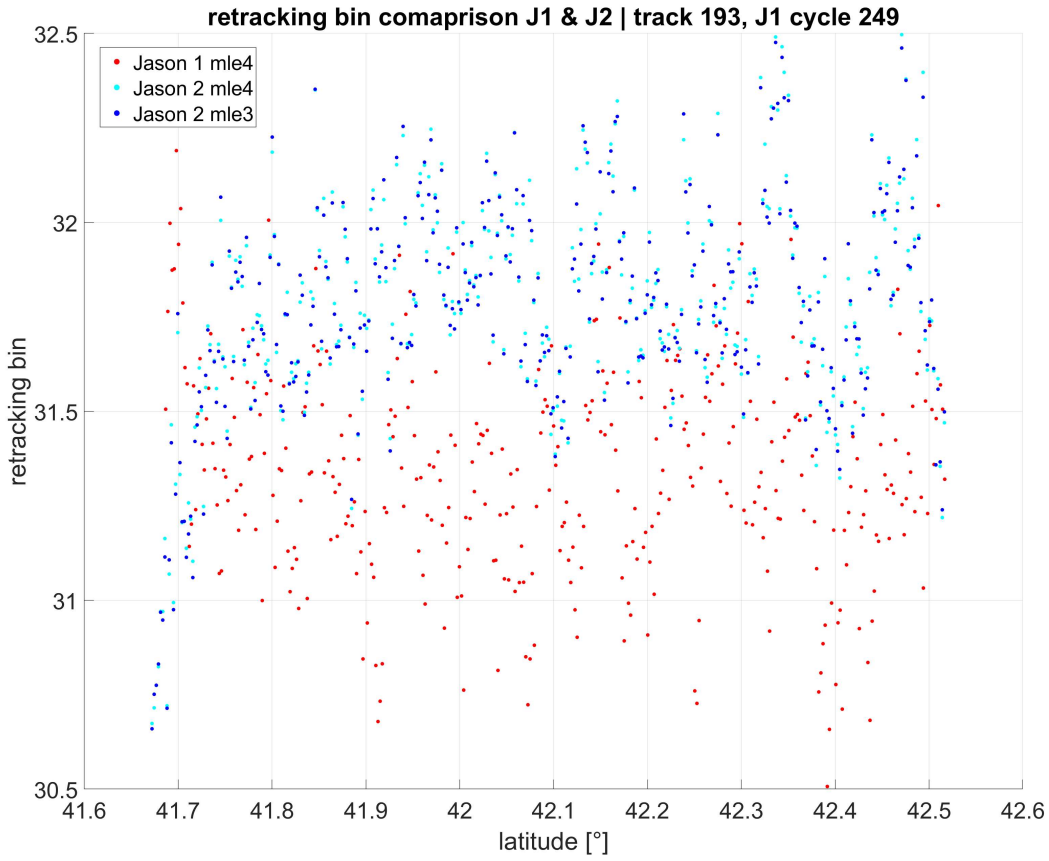

Figure 4.8: *The graphic shows the retracking points of Jason 1 and Jason 2. These are the same points as in Figure 4.7, in better presentation to be compared.*

After comparing Jason and Jason 2 during their tandem phase, the same procedure is done with Jason 2 and Jason 3 during their tandem phase.
Here are as well differences visible, between Jason 2 and Jason 3. In Figure 4.9 the retracking bins on a radargram are shown. Figure 4.10 shows the same bins, but with a better visual comparability. In the Table 4.7 the mean, median and standard deviations (std) of the retracking bins of Jason 2 MLE3 & MLE4 and Jason 3 MLE3 & MLE4 are listed. The maximal difference of the means is 0.412 bins, between Jason 2 MLE4 and Jason 3 MLE3. For the medians the maximal difference is 0.406 bins, between Jason 2 MLE4 and Jason 3 MLE3. The standard deviations are smaller compared to the standard deviations in Table 4.6. They are varying between 0.255 bins and 0.263 bins, compared to 0.280 to 0.289 bins. In general the differences between the retracking algorithms of one satellite are quite small. The biggest difference there is at the medians of Jason 3 MLE3 and MLE4 with 0.012 bins. This is three times bigger than the second biggest difference between the retracking algorithms.
The results here are similar to the results of the comparison between Jason 1 and Jason 2.

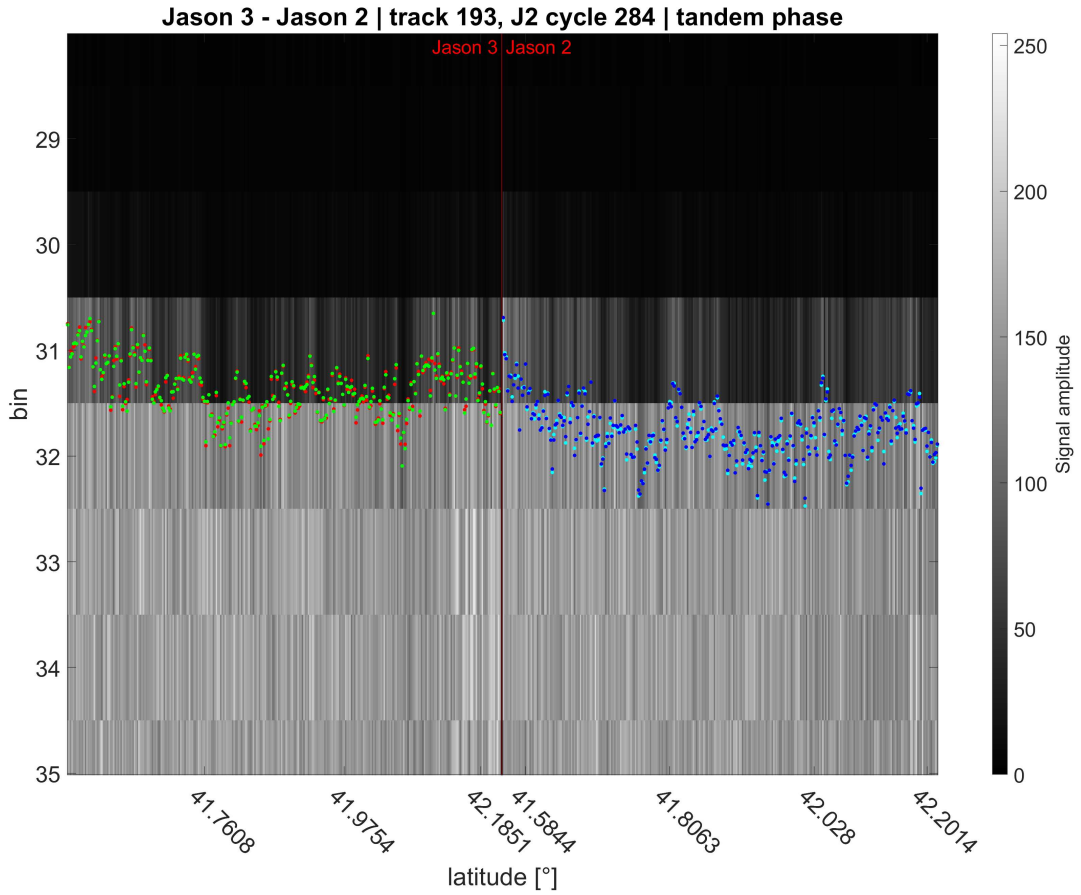

Figure 4.9: *The figure is showing cutouts of the waveforms reflected from Lake Erie, during the tandem phase of Jason 2 and Jason 3. It shows cutouts of one overflight over Lake Erie (track 193). The brightness symbolises the signal amplitude. The graphic is divided by the red line. On left are the waves of Jason 3, on the right are the waves from Jason 2. The x-axis shows the total number of waves. The red and green points are the retracked points of Jason 3, MLE4 and MLE3. The blue and cyan ones are the retracking points, MLE3 and MLE4, of Jason 2.*

Table 4.7: *The table is showing the mean, median and the standard deviation (std) of the retracking bins of track 193 from Jason 2 cycle 284 and Jason 3 cycle 004. The bins are also visualized in the Figure 4.9 and 4.10*

	mean [bin]	median [bin]	std [bin]
Jason 2 MLE4	31.759	31.758	0.263
Jason 2 MLE3	31.755	31.756	0.257
Jason 3 MLE4	31.351	31.364	0.261
Jason 3 MLE3	31.347	31.352	0.255

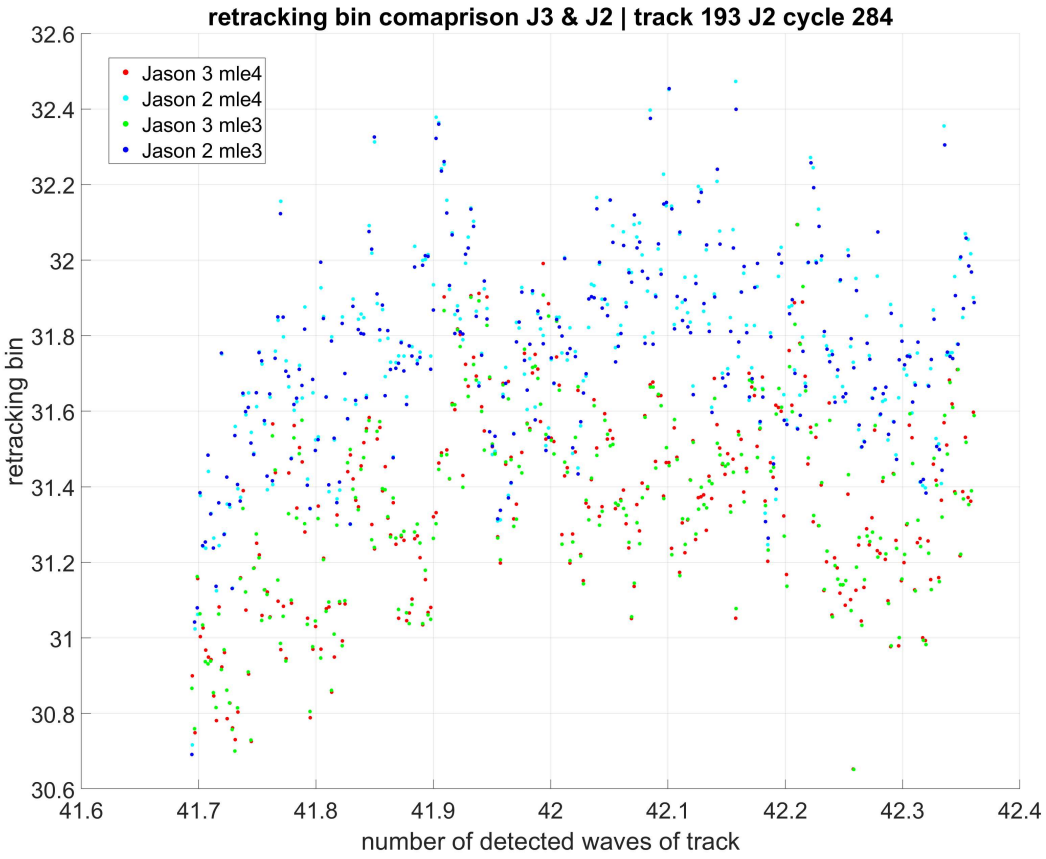

Figure 4.10: *The graphic shows the retracking points of Jason 2 and Jason 3. These are the same points as in Figure 4.9, in better presentation to be compared.*

Since a difference between Jason 1 and 2 or Jason 2 and 3 is ascertained during one pass of Lake Erie, another investigation is done to validate these results. The retracking algorithms try to find the point at the mid-height of the leading edge (Rosmorduc et al., 2011). In order to compare their results, the location of the retracking point and leading edge has to be determined. With a simple one dimensional interpolation the location with respect to the maximum can be estimated. For the leading edge, the first peak of the waveform, which is greater than 100, is chosen. In case the first peak is not the highest one and the retracking point is higher, the highest peak of the waveform is used. Now, the retraking point height compared to the peak height, in percentage, is determined. This is done for every measurement over Lake Erie during the tandem phase of Jason 2 and Jason 3. The results are separated by track number and shown in the Figure 4.11, 4.12 and 4.13.

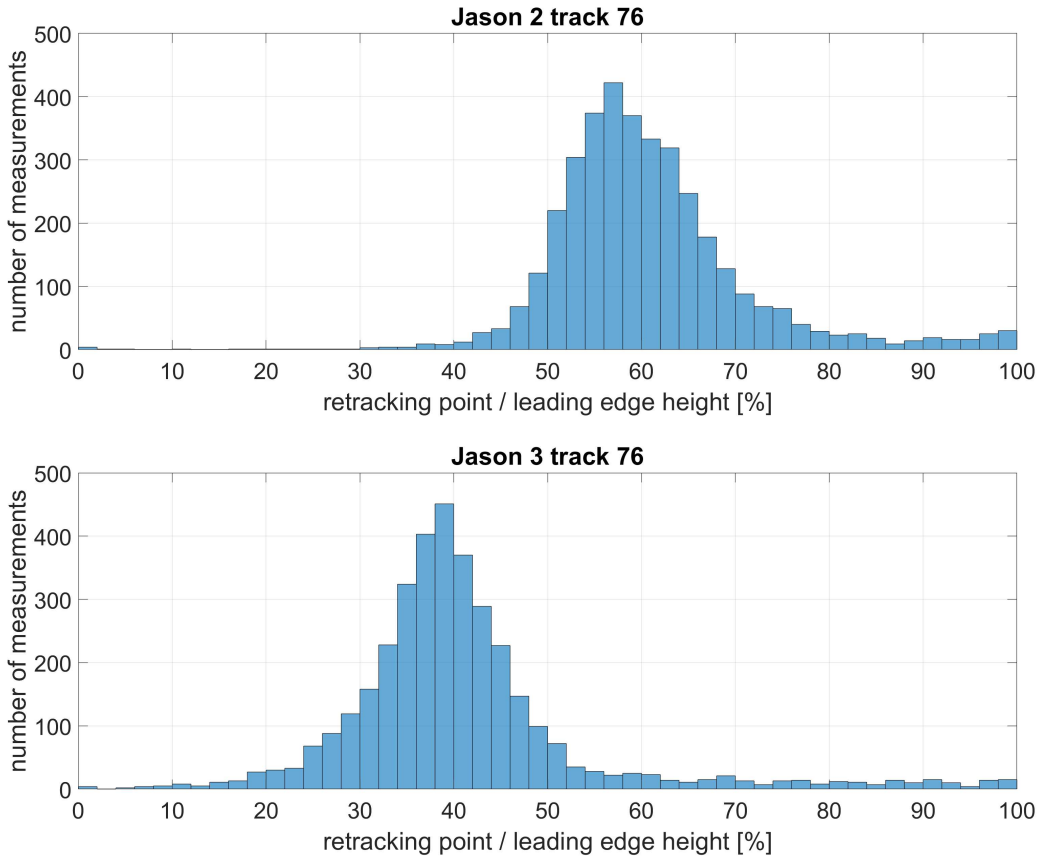

Figure 4.11: *The two histograms display the location of the retracking point, with respect to the leading edge, in percentage. The leading edge is defined as the first peak, with an signal amplitude greater than 100, of the waveform. In the special case, that the the location of the retracking point is above the leading edge, the maximal peak of the waveform is used for the leading edge. Both plots are created by using MLE4 retracking. The histogram on the top, belongs to Jason 2. The histogram on the bottom, belongs to Jason 3. The Histograms are made of all measurements over Lake Erie, that are observed during the whole tandem phase of Jason 2 and Jason 3 at track 76.*

In Figure 4.11, the findings from track 76 are depicted. At Jason 2, the tallest bar falls within the range of 56% to 58%, representing 422 out of 3683 measurements, which is very close to the 50% mark. Approximately around 50%, specifically between 48% to 52%, there are 341 measurements. At the extreme ends, the distribution of measurements is uneven, with 195 measurements spanning from 80% to 100%, and a mere 14 measurements within the 0% to 30% range.
For Jason 3, the largest bar appears between 38% to 40%, accounting for 451 measurements out of 3546. Around 50%, within the 48% to 52% range, there are only 171 measurements. The lower ranges, from 0% to 20%, encompass 79 measurements. Between 60% and 100%, the measurements are relatively evenly distributed across 2% wide bars, amounting to a total of 251 measurements.

In Figure 4.12, the histograms for track 152 depict distributions similar to those observed in track 76. For Jason 2, the most prominent bar falls within the range of 56% to 58%, representing 376 measurements out of 2811. Around 50%, specifically between 48% to 52%, there are 289 measurements. In the higher range of 80% to 100%, there are 51 measurements, while only 1 measurement falls within the 0% to 30% range.
Regarding Jason 3, the largest bar occurs between 38% to 40%, comprising 369 measurements out of 2712. Around the 50% mark, within the 48% to 52% range, there are only 125 measurements. The lower ranges, from 0% to 20%, encompass 43 measurements. Between 60% and 100%, there are 75 measurements distributed across this range.

In Figure 4.13, the histograms representing track 193 display distributions that slightly differ from those observed in track 76 and track 152. For Jason 2, the largest bar is situated within the range of 72% to 74%, encompassing 880 measurements out of 9341. Around the 50% mark, specifically from 48% to 52%, there are only 80 measurements. In the higher range of 80% to 100%, there are 1749 measurements, while a mere 26 measurements fall within the 0% to 30% range.
Regarding Jason 3, the largest bar occurs between 50% to 52%, comprising 1060 measurements out of 8968. Around the 50% mark, within the 48% to 52% range, there are 2106 measurements. The lower ranges, from 0% to 20%, encompass 25 measurements. Between 60% and 100%, there are 1405 measurements distributed across this range.
The retracking algorithm notably performed well in identifying the mid-height for Jason 3 at track 193. However, for track 76 and track 152, it tended to determine points closer to the 40% mark. In contrast, for Jason 2 in track 76 and track 152, the results are just a few percentages below 60% and so, slightly above the mid-height point. Yet, for track 193, almost all identified points are situated above the mid-height.

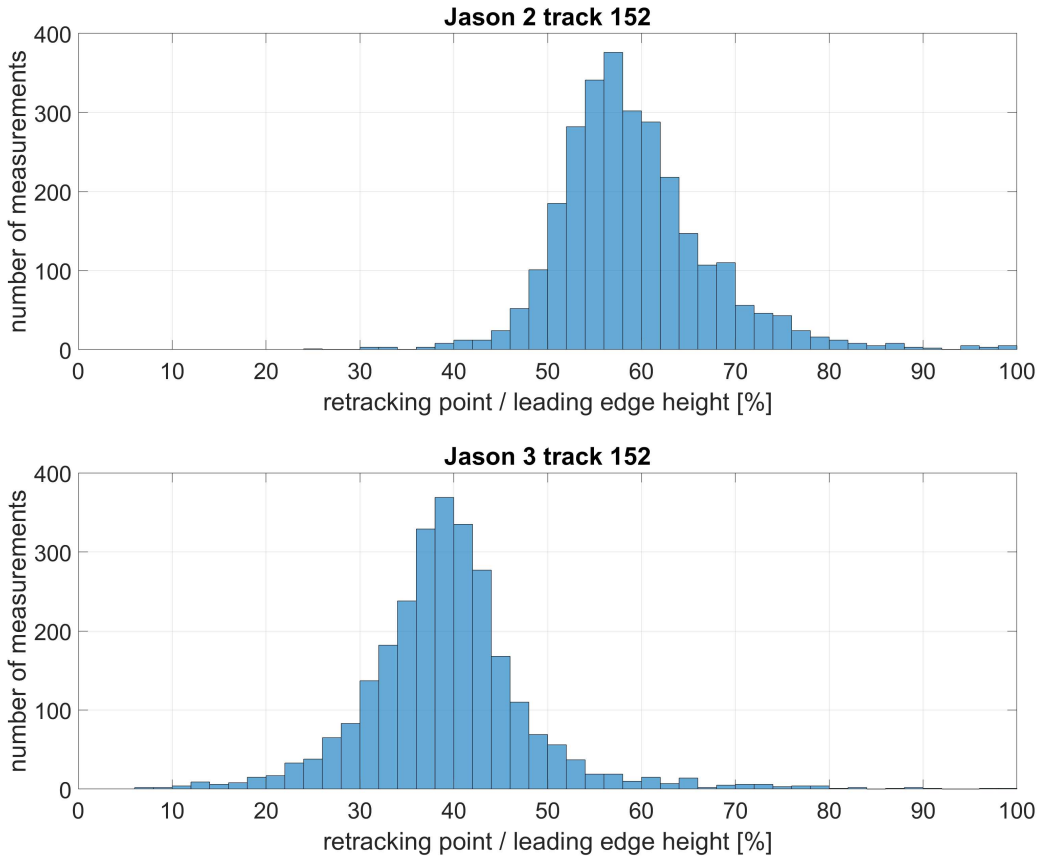

Figure 4.12: *The two histograms display the location of the retracking point, with respect to the leading edge, in percentage. The leading edge is defined as the first peak, with an signal amplitude greater than 100, of the waveform. In the special case, that the the location of the retracking point is above the leading edge, the maximal peak of the waveform is used for the leading edge. Both plots are created by using MLE4 retracking. The histogram on the top, belongs to Jason 2. The histogram on the bottom, belongs to Jason 3. The Histograms are made of all measurements over Lake Erie, that are observed during the whole tandem phase of Jason 2 and Jason 3 at track 152.*

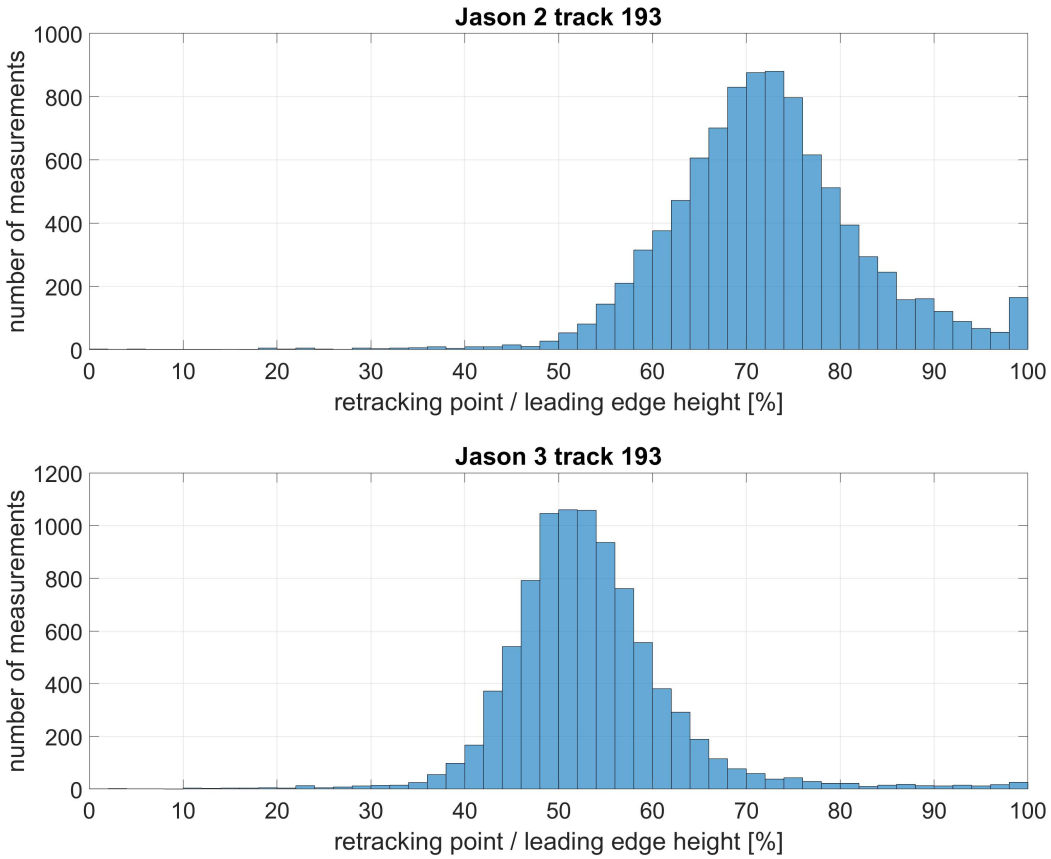

Figure 4.13: *The two histograms display the location of the retracking point, with respect to the leading edge, in percentage. The leading edge is defined as the first peak, with an signal amplitude greater than 100, of the waveform. In the special case, that the the location of the retracking point is above the leading edge, the maximal peak of the waveform is used for the leading edge. Both plots are created by using MLE4 retracking. The histogram on the top, belongs to Jason 2. The histogram on the bottom, belongs to Jason 3. The Histograms are made of all measurements over Lake Erie, that are observed during the whole tandem phase of Jason 2 and Jason 3 at track 193.*

The following Figure 4.14 shows a boxplot of every histogram shown in Figure 4.11, 4.12 and 4.13. Looking at the medians, the red line inside the blue box, the same results as above are visible. For track 76 and track 152, it is close to 40% for Jason 2 and for Jason 3 it is near to 60%. At track 193 both are higher. Jason 2 is above 70% and Jason 3 is near to 50%.
In all cases, the values of Jason 3 are lower than the results of Jason 2. Jason 3 is consistently around 20% lower in respect to the leading edge compared to Jason 2. Out of this data, it becomes clear that Jason 3 shows systematically lower values than Jason 2.

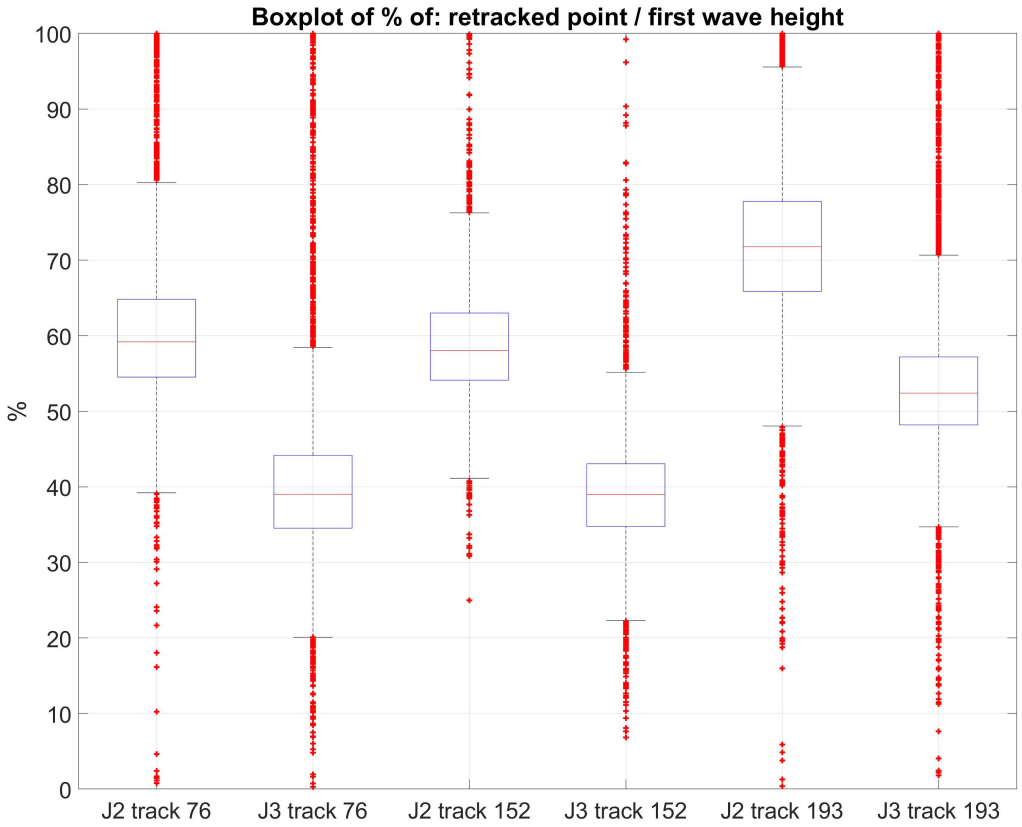

Figure 4.14: *The graphic is showing boxplots, one of each histogram shown in Figure 4.11, 4.12 and 4.13, of the percentages of the height of the retracking point from the first peak height (if its greater than 100%, the maximal peak height is used) of each wave. The top and bottom of each box are the 75th and 25th percentiles of the data. The red line inside the box is the median of the data. The Whiskers are the dotted lines from the box to the furthest observations. The red '+' are outliers* (Visualize summary statistics with box plot*, 2006).*

How far these aberrations, from the theory that requires the mid-height point, influence the LLH is yet unclear. In the following section a retracking algorithm is introduced that finds the midpoint of the leading edge.

4.1.1.1 Threshold retracking algorithm

In this section a threshold retracking algorithm, the so called *thr50*, is introduced. It is based one the theory that the retracking point should be at the mid-height of the leading edge. It will be tested if the bias can be reduced by using the mid-height point.

Methodology: thr50 is a very simple algorithm. In order to find the mid-height point, the leading edge must be defined. The height of the leading edge is defined as follows: First peak of each waveform, which has a signal amplitude larger than 100. This method is named *thr50f*.
Since the first peak is not always the highest peak, an alternative method is used. It defines the height of the leading edge as follows: Highest peak of the waveform. This method is named *thr50max*.
In Figure 4.15 an example waveform is shown. The first/max peak, how they are defined by *thr50f* and *thr50max*, are marked in red.

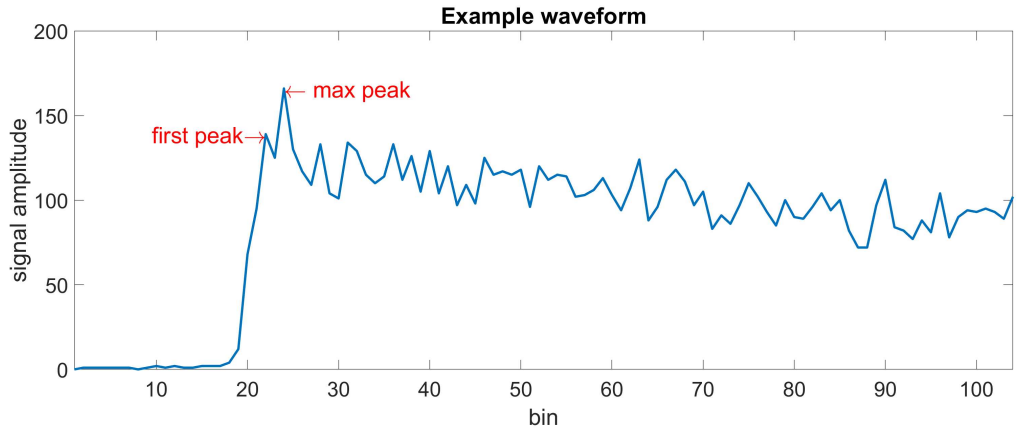

Figure 4.15: *Example of a waveform over Lake Erie from Jason 2. The first and max peak, as defined by thr50f and thr50max, are marked in red.*

With an one dimensional interpolation the retracking bin can be estimated. With equation (1.5) the range can be calculated. After replacing the range measurements, the LLH can be computed as normal.

Results: In order to see if there is a bias between Jason 2 and Jason 3, the LLH is computed for all the passes over Lake Erie at Jason 3 cycle 004. This is during the tandem phase of Jason 2 and Jason 3. The corrections from Jason 3 are used for Jason 2 as well.

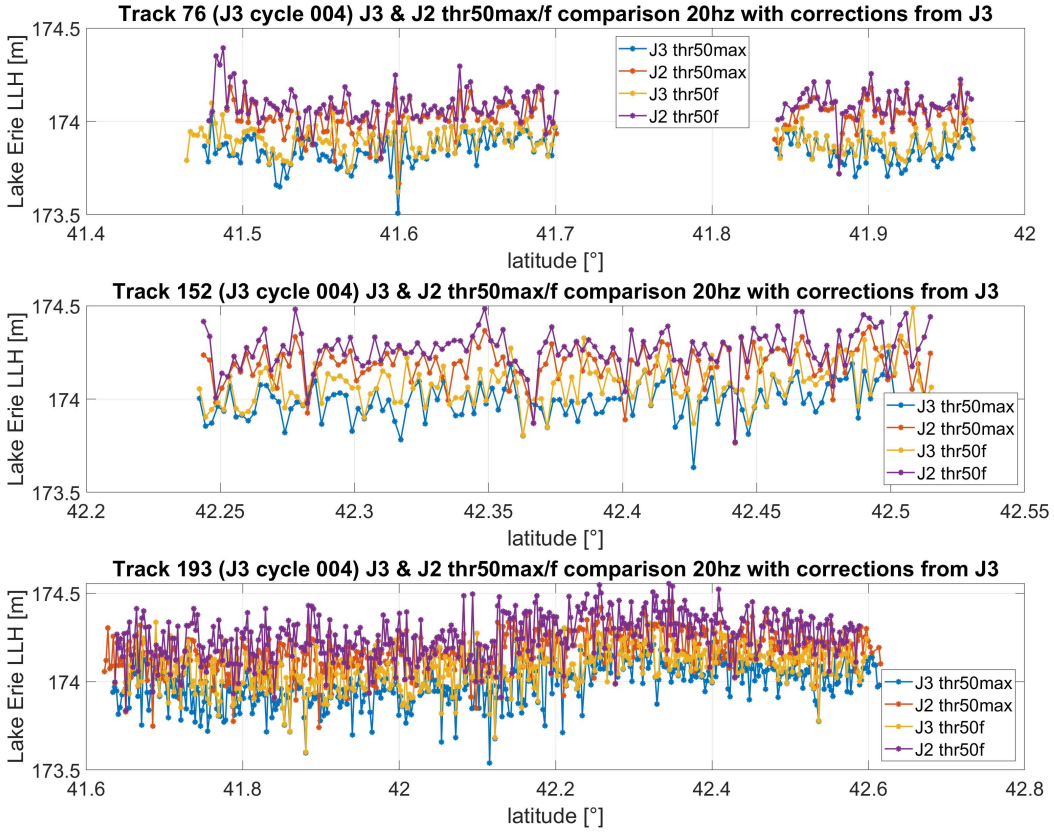

Figure 4.16: *LLH of Lake Erie during tandem phase of Jason 2 and 3, using thr50f and thr50max. LLH from Jason 3 cycle 004. For Jason 2 the same corrections from Jason 3 are used.*

In Figure 4.16 it is visible, at all three tracks, that thr50f and thr50max deliver different results. It also looks like that Jason 3 tend to measure lower LLH values than Jason 2. It can be observed that thr50f measures, at the median, around 5 to 9 cm higher values than thr50max. This indicates that in many cases the first peak is not the highest peak of the waveform.
The Table 4.8 shows the mean, median and standard deviation (std.) of the data shown in Figure 4.16. In the following the differences of the medians is viewed. The largest difference between thr50max and thr50f is at Jason 2 track 193, with −10.5 cm. The smallest difference between thr50max and thr50f is at Jason 2 track 76, with −4.9 cm. The largest difference between Jason 2 and Jason 3 with the same retracking algorithm, is at track 152 thr50f with 19.7 cm. The lowest difference is at the track 193 thr50f with 16.8 cm. The standard deviations are a bit higher compared to the ones in Table 4.10

and Table 4.12. Especially the track 193 stand out with standard deviations varying between ±11.8 cm and ±12.6 cm.

Table 4.8: *The table is showing the mean, median and standard deviation (std.) of the data shown in Figure 4.16.*

tracknumber	Mission	retracking	mean	median	std.
76	Jason 3	thr50max	173.847 m	173.843 m	7.9 cm
		thr50f	173.901 m	173.901 m	7.3 cm
	Jason 2	thr50max	174.022 m	174.028 m	8.7 cm
		thr50f	174.086 m	174.077 m	8.7 cm
152	Jason 3	thr50max	173.993 m	173.995 m	9.7 cm
		thr50f	174.083 m	174.079 m	11.6 cm
	Jason 2	thr50max	174.185 m	174.191 m	10.4 cm
		thr50f	174.267 m	174.276 m	11.3 cm
193	Jason 3	thr50max	173.989 m	173.991 m	11.9 cm
		thr50f	174.082 m	174.092 m	11.8 cm
	Jason 2	thr50max	174.161 m	174.165 m	11.6 cm
		thr50f	174.256 m	174.260 m	12.6 cm

All in all, it can be said that the differences between Jason 2 and Jason 3 could not be eliminated by using the mid-height point with the thr50 retracking algorithms. Thus, thr50f and thr50max have different results, the first peak is not the highest peak of the wave in most cases. In general the bias between the satellites increased up to 17 cm and more. Just by using the same corrections the bias reduced to a few centimeters or even less. Therefore, it can be said that the thr50 algorithms did not work out.

4.1.2 Investigating corrections

In this section the influence of the available corrections, in the geophysical data record (GDR), is investigated. Each satellite data is provided with its own set of corrections. Most corrections are provided by the same institutions. The idea is to use the provided corrections from one satellite also for another satellite and then compare the results. It is important that the satellites are measuring at the same locations and during the same time span. During the tandem phase of Jason 1 and Jason 2 (Jason 2 and Jason 3 as well) the satellites pass on the exact same orbit with approximately one Minute difference (*OSTM/Jason-2 Products Handbook*, 2017). Due to that spatial and temporal proximity it will be assumed that there are no significant changes in the atmosphere.
In Figure 4.17 some corrections of Jason 2 and 3 from track 193 are shown. The model dry troposphere corrections, both provided by ECMWF, do have a difference of approx. 5-8 cm above Lake Erie. Moreover a huge peak is visible near the northern end at Jason 2. The corrections value changes from -230 cm to nearly -160 cm. Meanwhile the correction value from Jason 3 does not change at all. The pole tide correction has some differences as well. At Lake Erie the difference is approx. -0.25 cm. It is also visible that the correction values have jumps in it. Other corrections exhibit minimal variations. However, considering the significant divergence in values provided by certain corrections, it is probable that there are issues within the computational models.

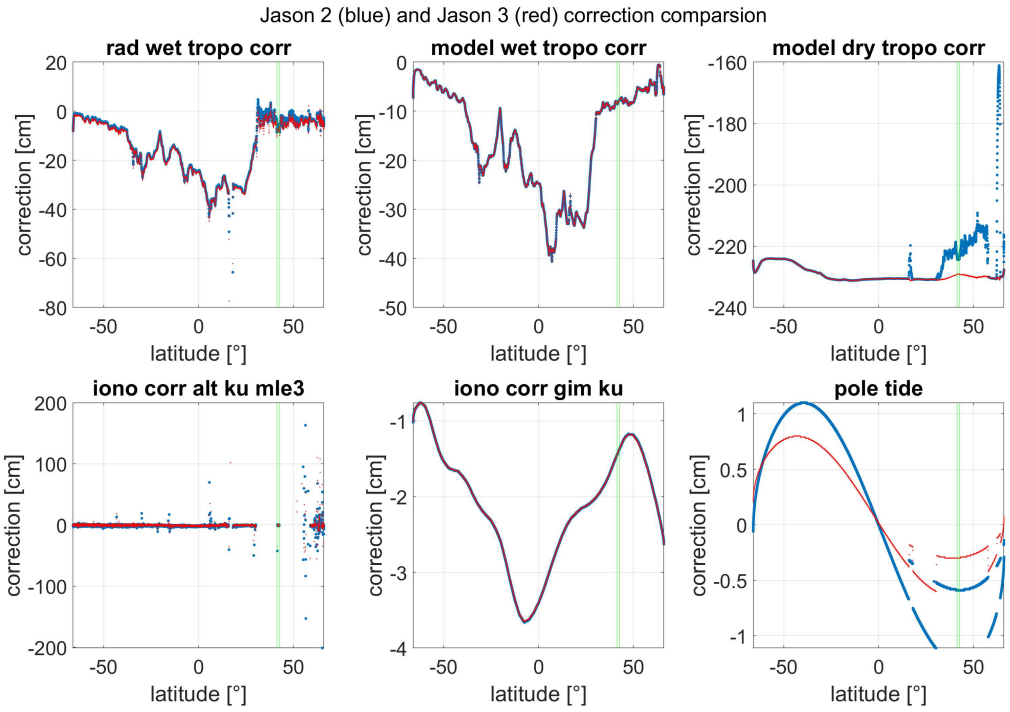

Figure 4.17: *Corrections provided from Jason 2 (blue) cycle 288 and Jason 3 (red) cycle 008 for track 193, GDR products. Between the two green lines Lake Erie is located.*

In the following, the corrections that are provided by Jason 1 GDR-E product are used also for Jason 2. This is applied only during the tandem phase. For comparison the same passes over Lake Erie as in Section 4.1 are used again.

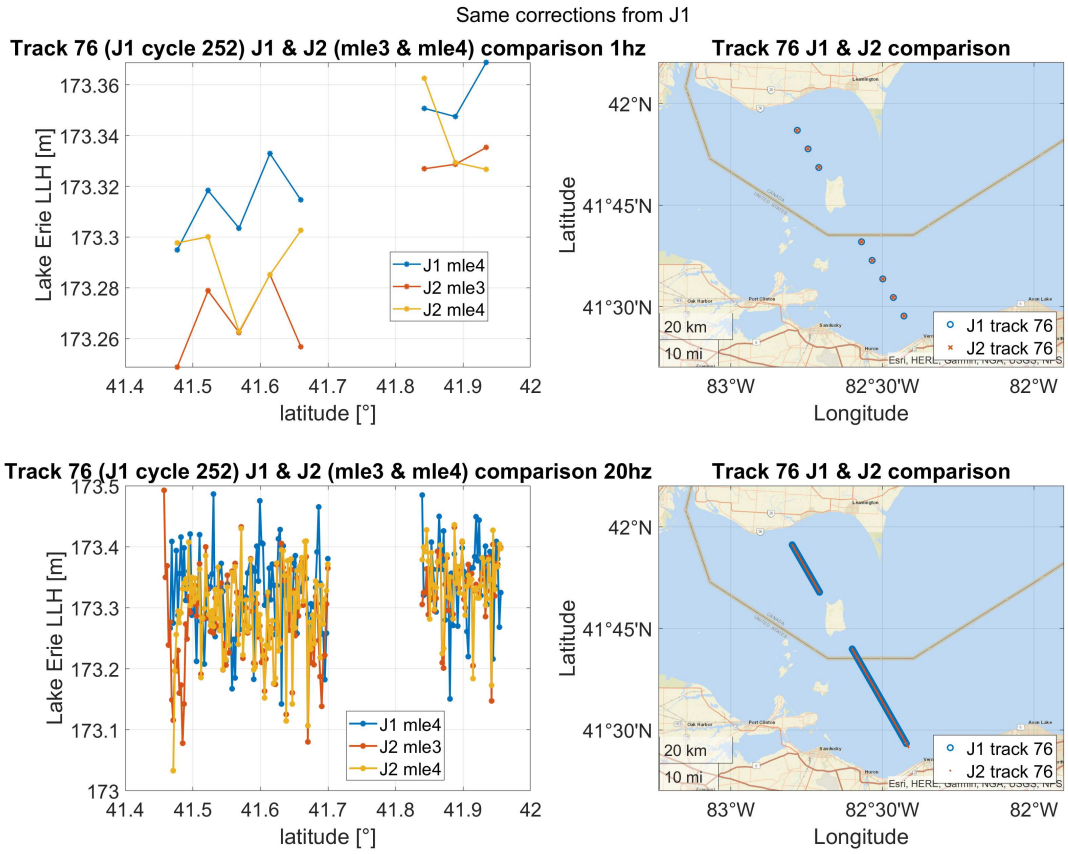

Figure 4.18: *Lake Erie LLH, Track 76 from Jason 1 cycle 252, Jason 2 cycle 013. On the top left are the reduced 1 Hz measurements, on the bottom left are the 20 Hz measurements. On the corresponding right side are maps that are showing the locations where the measurements are taken. The corrections which were used for Jason 1 and Jason 2, are from the Jason 1 GDR-E product.*

In Figure 4.18 the difference in the 1 Hz measurements seems to be bigger than in the 20 Hz measurements.
The 20 Hz measurements in Figure 4.19 look very similar. It is visible that the first measurements of Jason 2 deviate from those of Jason 1.

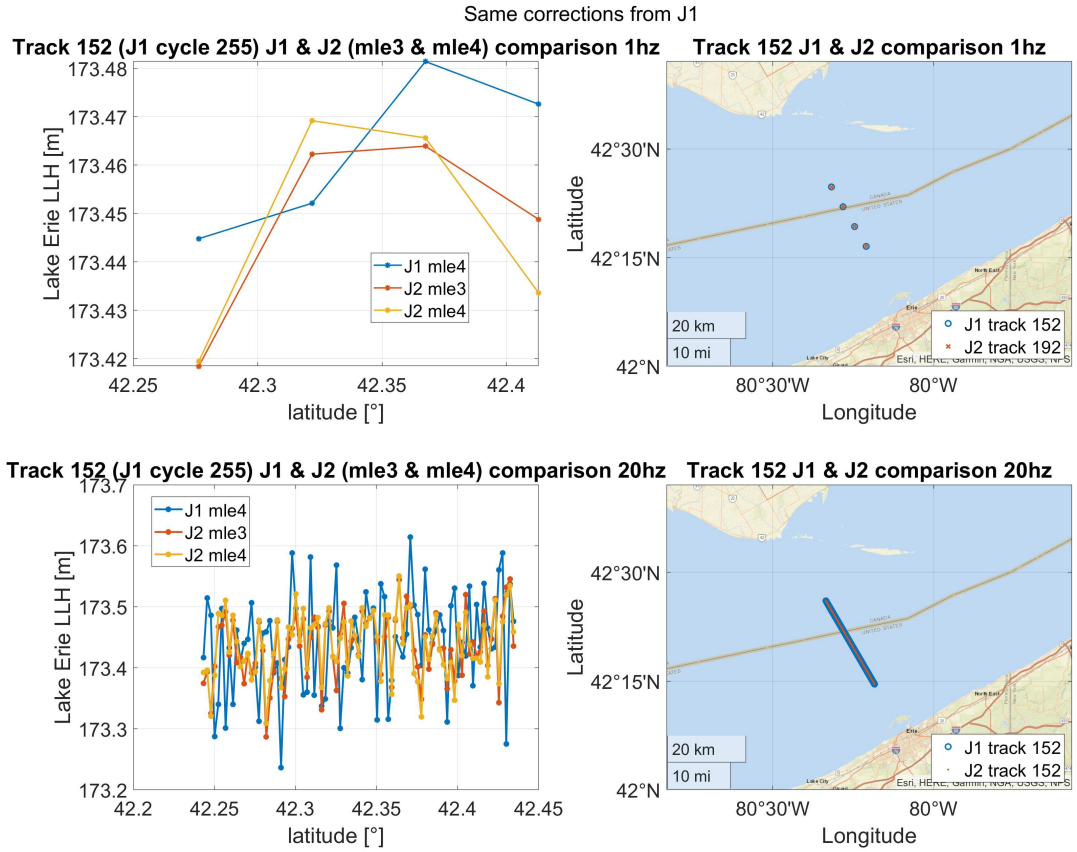

Figure 4.19: *Lake Erie LLH, Track 152 from Jason 1 cycle 255, Jason 2 cycle 016. On the top left are the reduced 1 Hz measurements, on the bottom left are the 20 Hz measurements. On the corresponding right side are maps that are showing the locations where the measurements are taken. The corrections which were used for Jason 1 and Jason 2, are from the Jason 1 GDR-E product.*

In the following, the values in the tables are being analyzed. Differences mentioned are always between the median values, unless otherwise is mentioned.
The Table 4.9 is showing the mean, median and standard deviation (std) of the 1 Hz data that are shown in the Figure 4.18, 4.19 and 4.20. The smallest difference is between Jason 1 MLE4 and Jason 2 MLE3, at track 152 with 0.6 cm. The largest difference is at track 76, between Jason 1 MLE4 and Jason 2 MLE3 with 4.4 cm. The difference between the two different retracking algorithms at Jason 2 is at minimum −0.4 cm and at maximum 1.9 cm.
Comparing those values to the ones in Table 4.2, one can see that the bias could be reduced.

Table 4.9: *Mean, median and standard deviation (std) of 20 Hz measurements, which are visualized in Figure 4.18, 4.19 and 4.20. For the measurements of Jason 2, the corrections from Jason 1 are used. At the column* ***Δmedian*** *the differences are always formed in the following order: Jason 1 - Jason 2 MLE4; Jason 1 - Jason 2 MLE3; Jason 2 MLE4 - Jason 2 MLE3. Acronyms: Jason 1 (J1), Jason 2 (J2), track (t.), cycle (c.)*

1 Hz	mean	median	std.	Δmedian
J1, MLE4, t.76, c.252	173.329 m	173.326 m	2.5 cm	+2.5 cm
J2, MLE4, t.76, c.013	173.308 m	173.301 m	3.1 cm	+4.4 cm
J2, MLE3, t.76, c.013	173.290 m	173.282 m	3.5 cm	+1.9 cm
J1, MLE4, t.152, c.255	173.463 m	173.462 m	1.7 cm	+1.2 cm
J2, MLE4, t.152, c.016	173.447 m	173.450 m	2.4 cm	+0.6 cm
J2, MLE3, t.152, c.016	173.448 m	173.456 m	2.1 cm	-0.6 cm
J1, MLE4, t.193, c.249	173.513 m	173.504 m	3.1 cm	-1.5 cm
J2, MLE4, t.193, c.010	173.522 m	173.519 m	4.3 cm	-1.9 cm
J2, MLE3, t.193, c.010	173.526 m	173.523 m	4.3 cm	-0.4 cm

The Table 4.10 is showing the mean, median and standard deviation (std) of the 20 Hz measurements that are shown in the Figure 4.18, 4.19 and 4.20. The largest difference between the two satellites is at track 76, between Jason 1 MLE4 and Jason 2 MLE3, with 2.9 cm and the smallest one is at track 193, between Jason 1 MLE4 and Jason 2 MLE3, with −0.1 cm. The difference between the two retracking algorithms of Jason 2 is minimal at track 152 and 193 with ±0.6 cm.

Table 4.10: *Mean, median and standard deviation (std) of 20 Hz measurements, which are visualized in Figure 4.18, 4.19 and 4.20. For the measurements of Jason 2, the corrections from Jason 1 are used. At the column* ***Δmedian*** *the differences are always formed in the following order: Jason 1 - Jason 2 MLE4; Jason 1 - Jason 2 MLE3; Jason 2 MLE4 - Jason 2 MLE3. Acronyms: Jason 1 (J1), Jason 2 (J2), track (t.), cycle (c.)*

20 Hz	mean	median	std.	Δmedian
J1, MLE4, t.76, c.252	173.332 m	173.335 m	6.6 cm	+1.7 cm
J2, MLE4, t.76, c.013	173.309 m	173.318 m	7.1 cm	+2.9 cm
J2, MLE3, t.76, c.013	173.294 m	173.306 m	7.6 cm	+1.2 cm
J1, MLE4, t.152, c.255	173.441 m	173.449 m	8.0 cm	+0.5 cm
J2, MLE4, t.152, c.016	173.439 m	173.444 m	5.2 cm	+1.1 cm
J2, MLE3, t.152, c.016	173.436 m	173.438 m	5.3 cm	+0.6 cm
J1, MLE4, t.193, c.249	173.521 m	173.521 m	7.3 cm	+0.5 cm
J2, MLE4, t.193, c.010	173.516 m	173.516 m	7.4 cm	-0.1 cm
J2, MLE3, t.193, c.010	173.521 m	173.522 m	7.2 cm	-0.6 cm

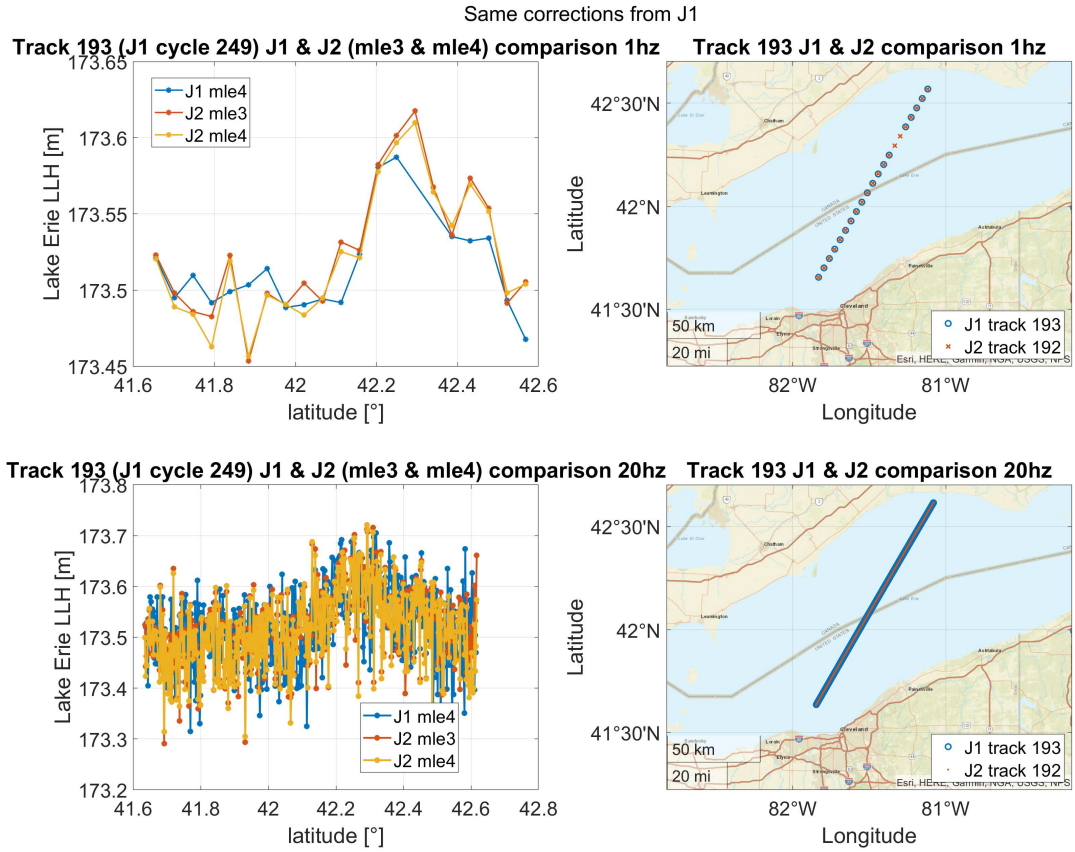

Figure 4.20: *Lake Erie LLH, Track 193 from Jason 1 cycle 249, Jason 2 cycle 010. On the top left are the reduced 1 Hz measurements, on the bottom left are the 20 Hz measurements. On the corresponding right side are maps that are showing the locations where the measurements are taken. The corrections which were used for Jason 1 and Jason 2, are from the Jason 1 GDR-E product.*

The same procedure is done with Jason 2 and Jason 3.

The following three Figure (Figure 4.21, Figure 4.22, Figure 4.23) visualizing the LLH measured by Jason 2 and Jason 3 during their tandem phase. The corrections from Jason 3, provided in the GDR-F product, are also used for Jason 2.

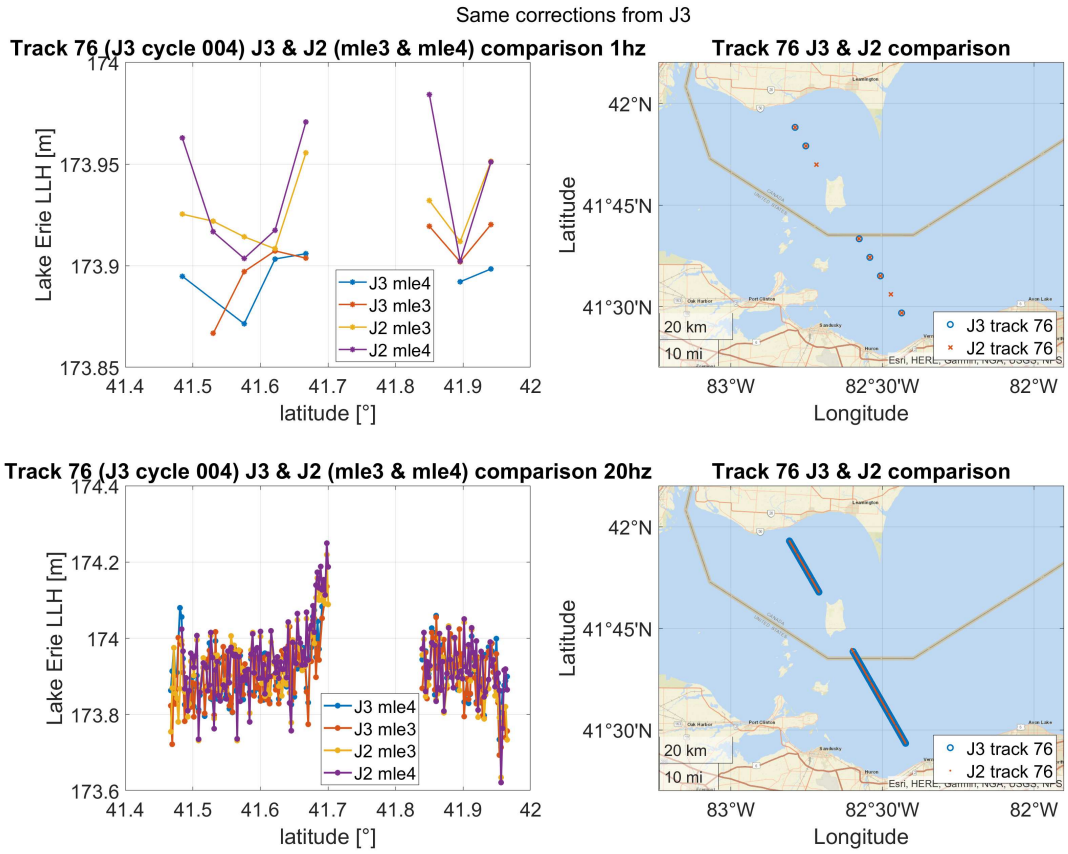

Figure 4.21: *Lake Erie LLH, Track 76 from Jason 2 cycle 284, Jason 3 cycle 004. On the top left are the reduced 1 Hz measurements, on the bottom left are the 20 Hz measurements. On the corresponding right side are maps that are showing the locations where the measurements are taken. The corrections which were used for Jason 3 and Jason 2, are from the Jason 3 GDR-F product.*

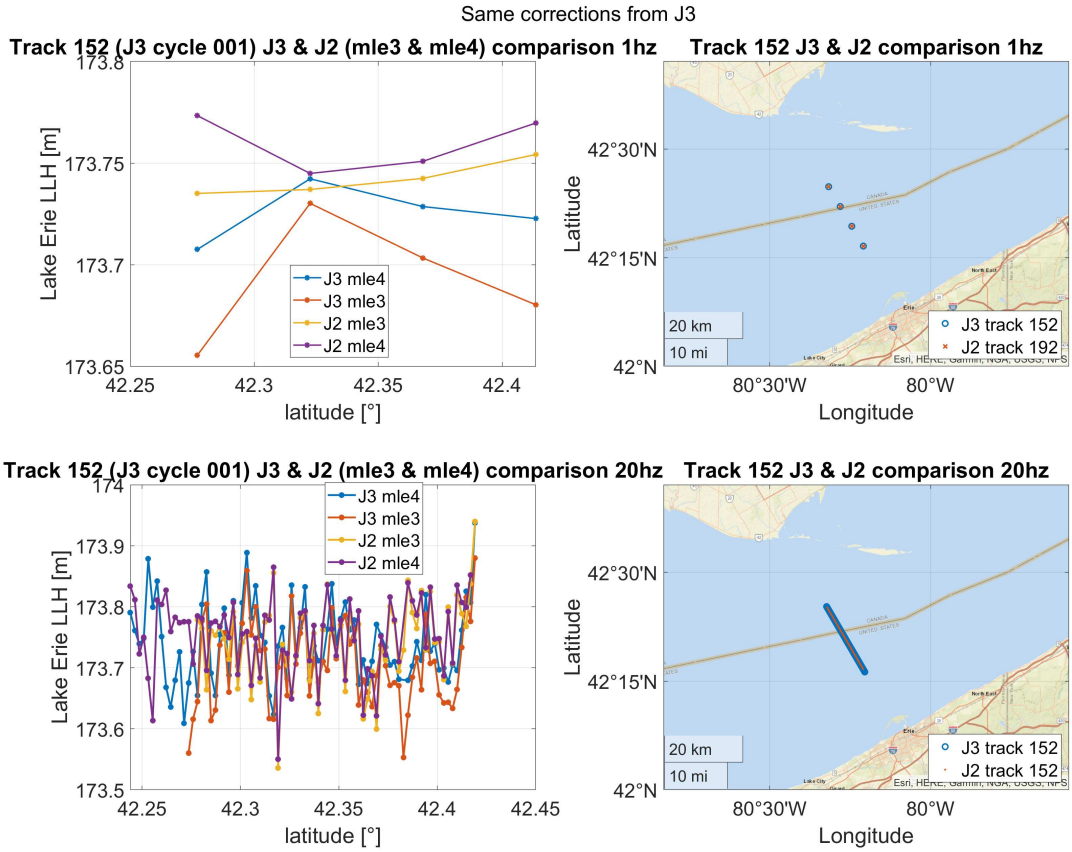

Figure 4.22: *Lake Erie LLH, Track 76 from Jason 2 cycle 281, Jason 3 cycle 001. On the top left are the reduced 1 Hz measurements, on the bottom left are the 20 Hz measurements. On the corresponding right side are maps that are showing the locations where the measurements are taken. The corrections which were used for Jason 3 and Jason 2, are from the Jason 3 GDR-F product.*

In the following, the values in the tables are being analyzed. Differences mentioned are always between the median values, unless otherwise is mentioned.
The Table 4.11 is showing the mean, median and standard deviation (std) of the 1 Hz data shown in the Figures 4.4, 4.5 and 4.6. The smallest difference between Jason 2 and the reference is at track 193 Jason 2 MLE3 with −0.1 cm and the largest is at track 152 Jason 2 MLE4 with 6.8 cm. Comparing the differences between the two retracking algorithms of one satellite, the smallest difference is at track 193 with 0.2 cm for Jason 3 and as well for Jason 2 with 0.5 cm. The largest difference is at track 152 for Jason 3 with 3.4 cm and at track 152 for Jason 2 as well, with 2.0 cm.

Table 4.11: *Mean, median and standard deviation (std) of 20 Hz measurements, which are visualized in Figures 4.4, 4.5 and 4.6. For the measurements of Jason 2, the corrections from Jason 3 are used. Jason 3 MLE4 serves as the reference mission for the differences. Acronyms: Jason 3 (J3), Jason 2 (J2), track (t.), cycle (c.)*

1 Hz	mean	median	std.	Δmedian
J3, MLE4, t.76, c.004	173.894 m	173.904 m	1.2 cm	-
J3, MLE3, t.76, c.004	173.902 m	173.897 m	1.8 cm	-0.7 cm
J2, MLE4, t.76, c.284	173.939 m	173.934 m	3.2 cm	3.1 cm
J2, MLE3, t.76, c.284	173.928 m	173.924 m	1.8 cm	2.0 cm
J3, MLE4, t.152, c.001	173.725 m	173.692 m	1.4 cm	-
J3, MLE3, t.152, c.001	173.692 m	173.726 m	3.2 cm	3.4 cm
J2, MLE4, t.152, c.281	173.760 m	173.760 m	1.4 cm	6.8 cm
J2, MLE3, t.152, c.281	173.742 m	173.740 m	0.9 cm	4.8 cm
J3, MLE4, t.193, c.008	173.213 m	173.209 m	6.0 cm	-
J3, MLE3, t.193, c.008	173.209 m	173.211 m	6.0 cm	0.3 cm
J2, MLE4, t.193, c.288	173.215 m	173.213 m	5.5 cm	0.4 cm
J2, MLE3, t.193, c.288	173.217 m	173.208 m	5.3 cm	-0.1 cm

When looking at the median values from Table 4.12, the smallest difference between Jason 2 and the reference is at track 193 Jason 2 MLE3 with 1.0 cm and the largest is at track 152 Jason 2 MLE4 with 2.9 cm. Comparing the differences between the two retracking algorithms of one satellite, the smallest difference is at track 193 with 0.1 cm for Jason 3 and as well as for Jason 2. The largest difference is at track 152 for Jason 3 with 3.3 cm and at track 152 for Jason 2 as well, with 1.5 cm.

Table 4.12: *Mean, median and standard deviation (std) of 20 Hz measurements, which are visualized in Figure 4.4, 4.5 and 4.6. For the measurements of Jason 2, the corrections from Jason 3 are used. Jason 3 MLE4 serves as the reference mission for the differences. Acronyms: Jason 3 (J3), Jason 2 (J2), track (t.), cycle (c.)*

20 Hz	mean	median	std.	Δmedian
J3, MLE4, t.76, c.004	173.912 m	173.910 m	6.9 cm	-
J3, MLE3, t.76, c.004	173.901 m	173.902 m	7.5 cm	-0.9 cm
J2, MLE4, t.76, c.284	173.938 m	173.931 m	9.1 cm	2.1 cm
J2, MLE3, t.76, c.284	173.924 m	173.921 m	8.8 cm	1.1 cm
J3, MLE4, t.152, c.001	173.743 m	173.739 m	6.5 cm	-
J3, MLE3, t.152, c.001	173.708 m	173.706 m	8.7 cm	-3.3 cm
J2, MLE4, t.152, c.281	173.753 m	173.768 m	6.2 cm	2.9 cm
J2, MLE3, t.152, c.281	173.743 m	173.753 m	6.8 cm	1.4 cm
J3, MLE4, t.193, c.008	174.204 m	174.204 m	8.4 cm	-
J3, MLE3, t.193, c.008	174.204 m	174.205 m	8.3 cm	0.1 cm
J2, MLE4, t.193, c.288	174.218 m	174.215 m	7.9 cm	1.1 cm
J2, MLE3, t.193, c.288	174.215 m	174.214 m	8.1 cm	1.0 cm

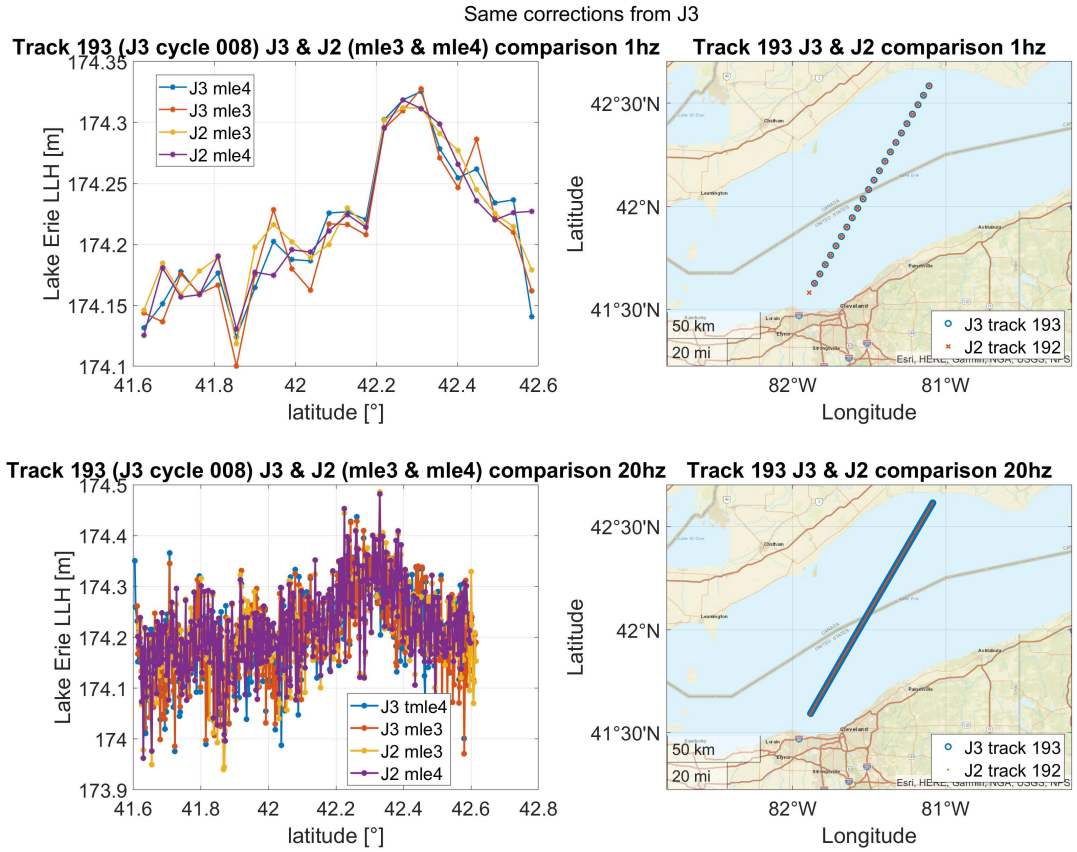

Figure 4.23: *Lake Erie LLH, Track 193 from Jason 2 cycle 288, Jason 3 cycle 008. On the top left are the reduced 1 Hz measurements, on the bottom left are the 20 Hz measurements. On the corresponding right side are maps that are showing the locations where the measurements are taken. The corrections which were used for Jason 3 and Jason 2, are from the Jason 3 GDR-F product.*

All in all, one can say that there are discrepancies in the provided corrections, as the bias could be reduced in a range of 0.2 cm to 11 cm by applying the same corrections for both satellites. This improvement was achieved during the tandem phases of both Jason 1 and 2, as well as between Jason 2 and 3. This shows, that it is vital to ensure that the corrections, applied to different satellites, fit together.

Chapter 5

Summary and conclusions

Inland altimetry is a very powerful tool for monitoring the water level of lakes. With only one satellite, it is not possible to create long term data records of many lakes all around the globe. Therefore, multi-mission monitoring must be sought. However, combining different satellite missions faces some challenges as there is always a bias between them. For fixing the bias several approaches are investigated in this thesis:

- The crossover adjustment allows to compute radial errors that includes all unconsidered errors. A cross-over adjustment over the ocean is performed. As an result the radial errors at the crossover points are estimated. Using them for inland altimetry, requires and extrapolation from ocean over land. The radial errors along a track, that goes over Lake Erie, are taken for the extrapolation, as well as the corresponding altitude of the satellite. Four extrapolation methods are tested. These are *linear*, *pchip*, *makima* and *spline*. *spline* was not used later on, since it delivered the worst results. Removing the radial errors from the lake level height, shows that the bias between the Jason satellites can be reduced. An improvement could be achieved at the first chosen time period, which includes the satellites Jason 1, Jason 2 and ENVISAT, in 2008. The differences between Jason 1 and 2, without removing the radial errors, is 1.7 cm. With the three tested extrapolation methods (linear, pchip and makima) the differences changed to 1.0 cm to 3.2 cm. The bias between Jason 1/2 and ENVISAT could not be reduced. However, the bias increased to 29.7 cm, rising by 9.2 cm. Moving to the second chosen time period the bias removal of satellites Jason 2, 3, and SARAL/AltiKa was targeted. In this case, no reduction in the bias was achieved during this phase. Initially, the difference between Jason 2 and 3 measured 0.4 cm, but post radial error removal, it escalated significantly to a range between 38.0 cm and 43.5 cm. A notable increase, ranging from 13.7 cm to 15.1 cm, was observed between Jason 2 and SARAL/AltiKa. Regarding Jason 3 and SARAL/AltiKa, the initial difference stood at 3.4 cm but post radial error removal, it fluctuated between 3.3 cm and 25.4 cm.
- Investigations on the effect of retracking algorithms on the observed bias were also performed. In focus were the MLE3 and MLE4 retracking algorithms. It turns out that MLE3 and MLE4 deliver very similar retracking bins. A difference between the satellites could be found instead. The same retracking algorithm

delivers slightly different results at different satellites. This is shown for MLE4 at Jason 2 and Jason 3 during the tandem phase. The mid-height point of the leading edge could not be found properly. At Jason 2 the retracking bin height is approx. 20% height of the leading edge higher than the retracking bin height at Jason 3. The difference between Jason 2 and Jason 3 is at every track the same. Thus, Jason 3 is systematically lower than Jason 2.
With the simple threshold retracking algorithms thr50max and thr50f, which uses the mid-height point for calculating the new range "measurement", it was tested if the bias could be solved. thr50max uses the highest peak of the waveform and thr50f uses the first significant peak for calculating the mid-height point. The same corrections for Jason 2 and 3 where used, since a reduction of the bias can be achieved, as we will see later. thr50max is using the point with the strongest signal of the waveform. thr50f uses the point of the first peak with an signal amplitude greater than 100. thr50f tend to deliver ~ 5 to 9 cm larger values than thr50max. In general one can say that the bias could not be solved. The smallest difference between Jason 2 and Jason 3 is at track 193 thr50f with 16.8 cm. In comparison with the MLE3 and MLE4 retracking, the bias could be reduced there to approximately 1 cm by using the same corrections. The largest difference is at track 152 thr50f with 19.7 cm.

- One source of bias could be found in the corrections provided in the GDR products. As they seem to have big differences during the tandem phases of Jason 1 and 2 as well as Jason 2 and 3. During these tandem phases the satellites passes over the same location, only one minute apart. In such a short time span no drastic changes of the atmosphere should occur. All three tracks, track 76, 152 and 193, are investigated separately. Both, the 1 Hz and the 20 Hz measurements are compared. Comparing Jason 1 with Jason 2, the bias ranges from 3.0 cm to 12.9 cm. By using the corrections from Jason 3 also for Jason 2, the bias reduced to a range from 0.6 cm to 4.4 cm. A similarly result was achieved with the 20 Hz measurements. There, the bias was at first in a range from 1.7 cm to 13.1 cm. This is reduced to a range from 0.1 cm to 2.9 cm.
  During the tandem phase of Jason 2 and Jason 3, the bias could be reduced as well. For the 1 Hz measurements, the bias was in a range from 0.9 cm to 13.7 cm. This is reduced to range from 0.1 cm to 6.8 cm. For the 20 Hz measurements this method worked as well. The bias ranged from 0.4 cm to 10.3 cm and could be reduced to a range from 1.0 cm to 2.9 cm.

In conclusion, the investigation into mitigating biases between different satellite missions through crossover analysis did not work as expected. While radial error removal exhibited success in diminishing biases between Jason 1 and Jason 2, it did not work for Jason 3, ENVISAT or SARAL/AltiKa. Nevertheless, for achieving the best outcomes for Jason 1 and 2, the best extrapolations methods are *linear* and *pchip*. The subsequent phase involving satellites Jason 2, Jason 3, and SARAL/AltiKa showed no success in bias reduction. Thus, further investigations why the crossover analysis did not work should be done, since it is a powerful tool if it works properly.
A further finding I made is that Jason 3, using MLE4, finds systematically lower retrack-

ing bins compared to Jason 2. In how far this does influence the range measurement, and in the end the LLH, is not investigated. In order to investigate if the bias is caused by the retracking algorithms, the simple threshold retracking algorithms thr50f and thr50max are employed. As an outcome the bias between Jason 2 and 3 increased. Thus, one can conclude that proper retracking is vital for consistent measurements, as retracking algorithms can cause biases.
Lastly, a critical identification of errors within the corrections provided in the GDR products proved as a significant contributor to biases. Addressing these discrepancies by utilizing corrections from different satellite sources showcased notable success in reducing biases, indicating the pivotal role of accurate corrections in refining measurements. Thus, the same corrections should be used if possible, as during the tandem phases of the Jason satellites. The corrections should also be controlled in a way that inconsistencies of a few centimeters, under the same conditions, are detected.

Bibliography

1-D data interpolation (table lookup) (n.d.), MathWorks. From MATLAB documentation. Accessed in 12/2023.

Aviso+ (n.d.), 'Orbit', *Aviso+* .
URL: *https://www.aviso.altimetry.fr/en/missions/current-missions/saral/orbit-1.html*

Aviso+ (2022). Timeline of modern radar altimetry missions. (2022).
URL: *https://doi.org/10.24400/527896/A02-2022.001*

Benveniste, J. and Milagro, M. (2000), *ENVISAT RA-2 AND MWR PRODUCTS AND ALGORITHMS USER GUIDE*. Doc. No.: RA-TN-ESR-GS-0013.
URL: *https://earth.esa.int/eogateway/documents/20142/37627/ENVISAT+RA-2+and+MWR+Products+and+Algorithms+User+Guide.pdf/b5f31173-0fbe-97b6-2a7d-c7ebb6842686?version=1.1t=1610383266680*

Bosch, W., Dettmering, D. and Schwatke, C. (2014), 'Multi-mission cross-calibration of satellite altimeters: Constructing a long-term data record for global and regional sea level change studies', *Remote Sensing* **6**(3), 2255–2281.
URL: *https://www.mdpi.com/2072-4292/6/3/2255*

Calculate geoid height (n.d.), MathWorks. From MATLAB documentation. Accessed in 11/2023.

Envisat Overview (n.d.). esa Envisat/Mission/Envisat overview no autho nor date.
URL: *https://earth.esa.int/eogateway/missions/envisat/description*

Fu, L. and Cazenave, A. (2000), *Satellite Altimetry and Earth Sciences: A Handbook of Techniques and Applications*, ISSN, Elsevier Science.
URL: *https://books.google.de/books?id=vMu29usEgb0C*

Jason-1 Products Handbook (2016).
URL: *https://www.aviso.altimetry.fr/fileadmin/documents/data/tools/hdbk_j1_gdr.pdf*

Jason-3 Products Handbook (2021).
URL: *https://www.aviso.altimetry.fr/fileadmin/documents/data/tools/hdbk_j3.pdf*

OSTM/Jason-2 Products Handbook (2017).
URL: *https://www.ospo.noaa.gov/Products/documents/hdbk_j2.pdf*

Rosmorduc, V., Benveniste, J., Lauret, O., Maheu, C., Milagro, M. and Picot, N. (2011), 'Radar altimetry tutorial', *ESA, Europe* pp. 112–128.

SARAL/AltiKa Products Handbook (2021). CNES, ISRO.
URL: *https://www.aviso.altimetry.fr/fileadmin/documents/data/tools/SARAL_Altika_products_handbook.pdf*

Sentinel-3 SRAL Marine User Handbook (2017).

Tourian, M. J. (2013), *Application of spaceborne geodetic sensors for hydrology*.

Vignudelli, S., Kostianoy, A. G., Cipollini, P. and Benveniste, J. (2011), *Coastal altimetry*, Springer Science & Business Media.

Visualize summary statistics with box plot (2006), MathWorks. From MATLAB documentation. Accessed in 10/2023.

Wikipedia (2023), 'Lichtgeschwindigkeit — wikipedia, die freie enzyklopädie'. [Online; Stand 23. Oktober 2023].
URL: *https://de.wikipedia.org/w/index.php?title=Lichtgeschwindigkeitoldid=237556693*